Carrier Phase-Based Synchronization and High-Accuracy Positioning in 5G New Radio Cellular Networks

Shaoshuai Fan, *Member, IEEE*, Wei Ni, *Senior Member, IEEE*, Hui Tian, *Senior Member, IEEE*, Zhiqian Huang, and Rengui Zeng

***Abstract*— Inspired by excellent precision of carrier phase positioning, this paper presents a new carrier phase positioning technique for 5G new radio cellular networks with a focus on clock synchronization and integer ambiguity resolution. A carrier-phase based clock offset estimation method is first proposed to achieve precise clock synchronization among base stations, and proved to achieve the Cramér–Rao Lower Bound (CRLB) asymptotically. A fusion method is developed to fuse the estimated positions of a mobile station (MS) based on time-difference-of-arrival, with the estimated position changes based on the temporal changes of carrier phase measurements. While circumventing the integer ambiguities of the carrier phase measurements, the fusion method provides quality interim estimates of the MS positions, at which the measurements can be linearized to resolve the integer ambiguities. As a result, precise MS positions can be obtained based on the disambiguated carrier phase measurements. Numerical simulations show that the proposed carrier phase positioning can achieve a centimeter-level accuracy in wireless cellular networks.**

***Index Terms*— Carrier phase positioning, New Radio (NR), clock synchronization, integer ambiguity resolution.**

I. Introduction

AS COMPARED to earlier generations of cellular networks, reliable positioning techniques with sub-meter or even centimeter accuracies are anticipated in fifth-generation (5G) New Radio (NR) systems and beyond [1] for new applications, such as Industrial Internet-of-Things (IIoT) [2]–[4].

There are two typical categories of wireless positioning techniques, namely, range-based techniques [5] and non-range-based techniques [6], [7]. The non-range-based schemes usually rely on the connectivity between nodes or the fingerprints of wireless propagation environments, which need to exchange information between devices or survey and collect massive information before positioning. Among range-based positioning methods, Time-of-Arrival (ToA) has been extensively utilized, where ranges are measured based on the round-trip delay between a base station (BS) and a mobile station (MS) [8]. Time-Difference-of-Arrival (TDoA) [9]–[14] is another widely-used method, which is the difference between the ToAs to two synchronized BSs and eliminates the need for synchronizing the BSs and MS. In ToA/TDoA systems, only pseudo-ranges can be obtained, which contain the clock offset caused by clock misalignment [5]. Angle-of-Arrival (AoA) is another popular method, which requires the installation of antenna arrays [15], [16]. Because each of the schemes has its merits and limitations, several hybrid methods have been proposed to improve the positioning accuracy [16], such as hybrid ToA/AoA method [17], and hybrid TDoA/AoA method [18], [19].

Precise range measurements are the key to the accuracy of range-based positioning. For any positioning algorithms, the accuracy of the range-based methods depends heavily on the resolution of devices and the signal bandwidth [20], [21]. Typically, the ranges are measured based on code phase and carrier phase [22]. As of code phase detection, the receiver replicates the transmitted pseudo-random noise (PRN) code and shifts the replica until the maximum correlation is attained. The shift of the replica code corresponds to the ToA from the transmitter to the receiver [5]. As a consequence, the precision of the code phase detection depends on the length of each chip, and may not be accurate enough.

Different from the code phase detection, the carrier phase detection translates a carrier phase to a distance. Once the transmitted signal is captured by the receiver, it is locked by a phase lock loop (PLL) [23], [24]. As shown in Fig. 1, carrier phase measurements (in blue) include a fraction of a cycle and a number of complete cycles measured after the phase is locked [25], [26]. While the fractional part of the carrier phase can be tracked by the PLL, the integer number of complete cycles (in red) is unknown initially when the PLL gets locked and remains ambiguous [27]–[29]. The integer ambiguity needs to be precisely resolved, to allow the range to be precisely measured by the carrier phase detection. In this paper, we implement the carrier phase positioning in 5G NR cellular networks.

Carrier phase positioning has been utilized in Global Navigation Satellite System (GNSS), and can be divided into phase-difference-based and non-phase-difference-based categories. In the phase-difference-based category, one or more GNSS reference receiver stations need to be placed at known

Manuscript received February 14, 2021; revised June 9, 2021 and August 25, 2021; accepted September 30, 2021. Date of publication October 11, 2021; date of current version December 17, 2021. This work was supported in part by the National Natural Science Foundation of China under Grant 61801044 and in part by the Beijing Univ. of Posts and Telecommun.-China Mobile Research Institute Joint Innovation Center. The associate editor coordinating the review of this article and approving it for publication was S. Affes. *(Corresponding author: Shaoshuai Fan.)*

Shaoshuai Fan, Hui Tian, Zhiqian Huang, and Rengui Zeng are with the State Key Laboratory of Networking and Switching Technology, Beijing University of Posts and Telecommunications, Beijing 100876, China (e-mail: fanss@bupt.edu.cn).

Wei Ni is with the Data61, CSIRO, Marsfield, NSW 2122, Australia.

Color versions of one or more figures in this article are available at https://doi.org/10.1109/TCOMM.2021.3119072.

Digital Object Identifier 10.1109/TCOMM.2021.3119072

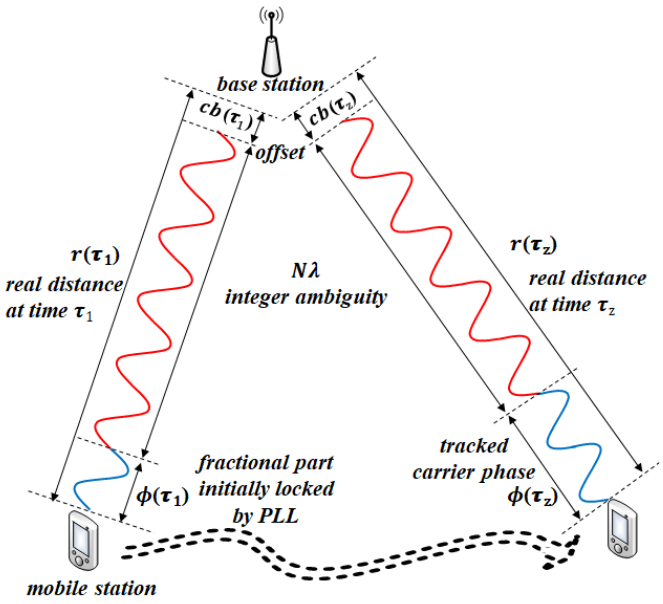

Fig. 1. An illustration of the carrier phase measurement for the localization of the MS. The initial integer number of complete cycles (in red) is unknown, and the receiver can keep tracking of the changes of its phase while recording the number of additional complete cycles (in blue) [23], [25], [27].

positions, and the distance between the reference station and the target terminal is significantly shorter than the orbit altitude of GNSS satellites [22]. By using differential carrier phase measurements, the common measurement errors caused by the propagation environment and clock bias can be eliminated. In the non-phase-difference-based category, neither reference stations nor additional observations are needed, but additional information is needed for linearizing the observation equations and resolving the integer ambiguity [30]. Therefore, dual frequency-based methods that linearly combine the frequencies of two GPS signals are usually applied [31]. Based on wide-lane or narrow-lane observations obtained by linear combination, a different wavelength of the carrier is generated, which can benefit the integer ambiguity resolution. The additional information can also be obtained by triple frequency-based methods with better wide- and narrow-lane information [32], [33] or multi-GNSS positioning techniques with various code and carrier phase observations [32], [34]. In summary, the integer ambiguity resolution process for real-time GNSS positioning needs either a baseline condition which requires reference stations to be placed nearby at known positions, or additional information generated by multiple carrier frequencies or joint measurements from multiple systems.

This paper presents a new carrier phase positioning technique to achieve sub-meter or even centimeter positioning accuracies in 5G NR cellular networks. The key contributions of the paper are summarized as follows:

- By taking into account the clock offset and integer ambiguity of carrier phase measurements, a high-accuracy carrier phase positioning problem is formulated as a nonlinear mixed-integer programming (NMIP) problem. We decouple the problem into a clock synchronization subproblem, and an integer ambiguity resolution and positioning subproblem.

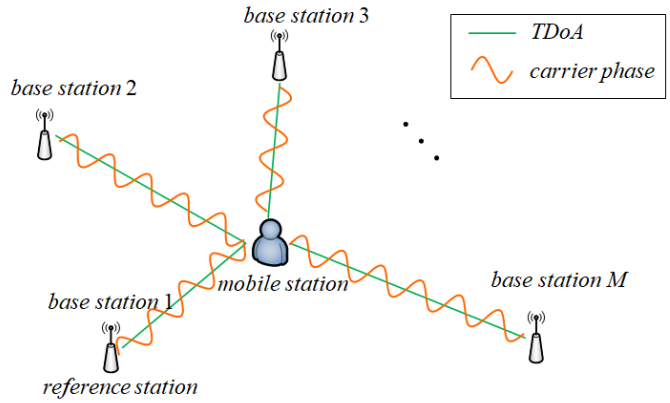

Fig. 2. Carrier phase positioning scenario of wireless cellular networks.

- A new carrier phase-based clock offset estimation method is proposed to achieve precise clock synchronization among BSs through wireless measurements, and proved to achieve the Cramér–Rao Lower Bound (CRLB) asymptotically.
- A new fusion method is developed to fuse the estimated positions of an MS based on TDoA, and the estimated position changes of the MS based on the temporal changes of the carrier phase measurements. By this means, we circumvent the integer ambiguities of the carrier phase measurements and obtain quality interim position estimates.
- Given the quality interim position estimates, the carrier phase measurements can be effectively linearized to resolve the integer ambiguities. As a result, precise MS positions with centimeter accuracies can be obtained based on the disambiguated carrier phase measurements.

It is worth mentioning that the concept of carrier phase positioning was first proposed for 5G NR systems in [35], where continuous positioning reference signals were designed. This paper is the first to provide a complete procedure of carrier phase positioning in wireless cellular networks with a focus on the challenging clock synchronization and integer ambiguity resolution.

The rest of this paper is organized as follows. Section II describes the system model and the proposed procedure of carrier phase positioning. Section III formulates the problem of clock synchronization, integer ambiguity resolution and positioning, and provides an overview of the proposed solution. Section IV presents the new carrier phase based clock offset estimation method to precisely synchronize the BSs. Section V resolves the integer ambiguity of carrier phase measurements to accurately estimate the positions of the MS. Section VI evaluates comprehensively the proposed carrier phase positioning approach through simulations, followed by conclusions in Section VII.

II. System Model of Carrier Phase Positioning

Suppose that there are M BSs at known positions and an MS to be located, as shown in Fig. 2. The i-th BS is located at $\boldsymbol{\zeta}_i = [A_i, B_i, C_i]^\dagger$. The subscript "$\dagger$" stands for transpose. At time t, the MS is situated at $\boldsymbol{\theta}(t) = [x(t), y(t), z(t)]^\dagger$ within the communication range of all the M BSs. The distance

between BS i and the target MS is given by

$$r_i(t) = \|\boldsymbol{\zeta}_i - \boldsymbol{\theta}(t)\|_2 = \sqrt{(A_i - x(t))^2 + (B_i - y(t))^2 + (C_i - z(t))^2}, \quad (1)$$

where $\|\cdot\|_2$ takes Euclidean norm.

The distance differences of the MS are measured between the BSs, based on TDoA and carrier-phase-difference-of-arrival (CPDoA). BS 1 serves the reference station. Based on the TDoA measurements, the distance difference of the MS between BSs i and 1 at time t, denoted by $D_{i1}(t)$ (in meters), is given by

$$D_{i1}(t) = r_{i1}(t) - c\delta_{i1}(t) + n_{i1}^{td}(t), \quad (2)$$

where $r_{i1}(t) = r_i(t) - r_1(t)$ is the actual distance difference between BSs i and 1; c is the speed of light; $b_i(t) = o_i(t) - o_{MS}(t)$ is the clock offset between BS i and the MS; $o_i(t)$ and $o_{MS}(t)$ are the clocks of BS i and MS, respectively; $\delta_{i1}(t) = b_i(t) - b_1(t) = o_i(t) - o_1(t)$ (in seconds) is the clock offset between the BSs with the clock offset of the MS $o_{MS}(t)$ canceled; and $n_{i1}^{td}(t)$ is the zero-mean additive white Gaussian ranging error with the variance of σ_{td}^2, resulting from the TDoA measurement noise.

The MS also transmits reference signals for uplink carrier phase positioning [35], [36]. Three types of signals have been discussed in 3GPP and can be potentially used as the reference signals for positioning [36]: (a) Sounding reference signal (SRS), which is an existing uplink NR reference signal and usually transmitted at a large interval, e.g., 0.5 ms [37]. (b) Enhanced SRS, which is transmitted using staggered patterns; in other words, the signals are transmitted on staggered subcarriers and continuous symbols [36]. The enhanced SRS has a narrow bandwidth and can be used as the reference for the phase lock loops of the receivers. (c) Carrier phase reference signal (C-PRS), which is a sinusoidal carrier signal at a pre-configured carrier frequency and can be used for carrier phase measurements in high-accuracy positioning applications that necessitate continuous tracking of UE positions [35]. The carrier phase lock loops are implemented at the BSs. At time t, the (ambiguous) distance measurement corresponding to the carrier-phase-of-arrival (CPoA) between BS i and the MS, denoted by $\phi_i(t)$ (in meters), is given by

$$\phi_i(t) = r_i(t) - N_i(t)\lambda - cb_i(t) + n_i^{ca}(t), \quad (3)$$

where $N_i(t)$ is an integer ambiguity resulting from the periodicity of phase; λ is the wavelength; and $n_i^{ca}(t)$ is the zero-mean Gaussian range error with the variance of σ_{ca}^2, resulting from the carrier phase measurement noise. In considered 5G New Radio scenario [38], the impact of multipath/not-line-of-sight (NLOS) is relatively benign, due to the quasi-optimal and sparse multi-path propagation properties of mmWave [39], [40]. We first assume that the PLL can correctly lock the carrier signal with no cycle slips. In other words, $N_i(t)$ remains unchanged over time, i.e., $N_i(t) = N_i$. We will generalize and validate the proposed technique in the presence of cycle slips in Sections V-D and VI.

By using CPDoA, the clock offset between the BSs and MS can be bypassed. The corresponding (ambiguous) distance difference measurement of the MS between BSs i and 1 at time t, denoted by $\phi_{i1}(t)$ (in meters), is given by

$$\phi_{i1}(t) = \phi_i(t) - \phi_1(t) = r_{i1}(t) - N_{i1}\lambda - c\delta_{i1}(t) + n_{i1}^{ca}(t), \quad (4)$$

where $N_{i1} = N_i - N_1$, and $n_{i1}^{ca}(t) = n_i^{ca}(t) - n_1^{ca}(t)$ is a zero-mean additive white Gaussian noise with variance of $2\sigma_{ca}^2$.

We note that the TDoA-based distance difference measurements $D_{i1}(t)$ suffer from large variations, while the CPDoA-based distance difference measurements $\phi_{i1}(t)$ are biased due to the integer ambiguity and undergo small variations [41]. In other words, $\sigma_{ca}^2 \ll \sigma_{td}^2$, and the carrier phase measurements can significantly improve the positioning accuracy if the integer ambiguity and the time-varying clock offset in (4) can be precisely estimated and suppressed.

Clock synchronization between the BSs is critical to the positioning. To accurately synchronize the BSs (e.g., with a nanosecond or sub-nanosecond accuracy), a BS can measure the ToA and CPoA from the other BSs based on positioning reference signals. The ToA-based distance measurement between BSs i and 1 at time t, denoted by $T_{i1}(t)$ (in meters), is given by

$$T_{i1}(t) = d_{i1} - c\delta_{i1}(t) + n_{i1}^{toa}(t), \quad (5)$$

where d_{i1} is the distance between BSs i and 1, and $n_{i1}^{toa}(t)$ is the zero-mean additive white Gaussian range error with the variance of σ_{toa}^2, resulting from the ToA measurement noise.

The CPoA-based distance measurement between the BSs, denoted by $\psi_{i1}(t)$ (in meters), is given by

$$\psi_{i1}(t) = d_{i1} - \mathcal{N}_{i1}\lambda - c\delta_{i1}(t) + n_{i1}^{ca}(t), \quad (6)$$

where $\mathcal{N}_{i1}$ is the integer ambiguity due to the periodicity of phase; $n_{i1}^{ca}(t)$ is the zero-mean additive white Gaussian range error with the variance of σ_{ca}^2, resulting from the CPoA measurement noises; and $\sigma_{toa}^2 \gg \sigma_{ca}^2$.

Suppose that the BS locks the carrier phase using its PLL, and records the carrier phase measurements from time t_0 to time t_K. Given the integer ambiguity of a link $\mathcal{N}_{i1}$ is independent of the clock offset δ_{i1}, we can eliminate the ambiguity of $\mathcal{N}_{i1}$ by evaluating the temporal change of the CPoA-based measurements between BSs i and 1 (referred to as "time-differential CPoA-based distance measurement") from time t_0 to time t, i.e., $\psi_{i1}(t) - \psi_{i1}(t_0)$, as given by

$$\Delta\psi_{i1}(t) = \psi_{i1}(t) - \psi_{i1}(t_0) = -c(\delta_{i1}(t) - \delta_{i1}(t_0)) + n_{i1}^{ca}(t) - n_{i1}^{ca}(t_0). \quad (7)$$

Let $\mathbf{D} = \{d_{i1}(t)\}_{(M-1)\times Z}$ and $\phi = \{\phi_{i1}(t)\}_{(M-1)\times K}$ collect the TDoA-based and the CPDoA-based distance difference measurements of the MS between BS 1 and the other BSs from time $t = \tau_1$ to $t = \tau_Z$, respectively. Also let $\mathbf{T} = \{T_{i1}(t)\}_{(M-1)\times K}$ collect the ToA-based distance measurements between BS 1 and the other BSs, and $\boldsymbol{\Psi} = \{\Delta\psi_{i1}(t)\}_{(M-1)\times K}$ collect the time-differential CPoA-based distance measurements (between BS 1 and the other BSs), from time $t = t_1$ to $t = t_K$.

III. Problem Formulation and Solution Overview

A. Problem Formulation

Given the ToA, TDoA, CPoA and CPDoA measurements, we use the maximum-likelihood estimation (MLE) to estimate the MS positions $\boldsymbol{\theta}$, the integer ambiguities of the CPDoA-based measurements $\mathbf{N}$, and the clock offsets between the BSs $\boldsymbol{\delta}$, as follows:

$$\max_{\boldsymbol{\theta}\in\mathbb{R},\mathbf{N}\in\mathbb{Z},\boldsymbol{\delta}\in\mathbb{R}} p(\mathbf{D},\boldsymbol{\phi},\mathbf{T},\boldsymbol{\Psi}|\boldsymbol{\theta},\mathbf{N},\boldsymbol{\delta}), \tag{8}$$

where the a-posteriori probability $p(\mathbf{D},\boldsymbol{\phi},\mathbf{T},\boldsymbol{\Psi}|\boldsymbol{\theta},\mathbf{N},\boldsymbol{\delta})$ is given by

$$\begin{aligned}
&p(\mathbf{D},\boldsymbol{\phi},\mathbf{T},\boldsymbol{\Psi}|\boldsymbol{\theta},\mathbf{N},\boldsymbol{\delta})\\
&=\prod_{i=2}^{M}\prod_{k=1}^{K}\frac{1}{\sqrt{2\pi}\sigma_{toa}}\exp\{-\frac{(T_{i1}(t_k)-d_{i1}+c\delta_{i1}(t_k))^2}{2\sigma_{toa}^2}\}\\
&\quad\times\prod_{i=2}^{M}\frac{1}{(2\pi)^{K/2}|\mathbf{Q}_\phi|^{1/2}}\\
&\quad\exp\{-\frac{1}{2}(\boldsymbol{\Psi}_{i1}+c\Delta\boldsymbol{\delta}_{i1})\mathbf{Q}_\phi^{-1}(\boldsymbol{\Psi}_{i1}+c\Delta\boldsymbol{\delta}_{i1})^\dagger\}\\
&\quad\times\prod_{z=1}^{Z}\frac{1}{(2\pi)^{(M-1)/2}|\mathbf{Q}_{td}|^{1/2}}\\
&\quad\exp\{-\frac{1}{2}(\mathbf{D}_z-\mathbf{r}_z+c\boldsymbol{\delta}_z)^\dagger\mathbf{Q}_{td}^{-1}(\mathbf{Q}_z-\mathbf{r}_z+c\boldsymbol{\delta}_z)\}\\
&\quad\times\prod_{z=1}^{Z}\frac{1}{(2\pi)^{(M-1)/2}|\mathbf{Q}_\phi|^{1/2}}\\
&\quad\exp\{-\frac{1}{2}(\boldsymbol{\phi}_z-\mathbf{r}_z+\mathbf{N}\lambda+c\boldsymbol{\delta}_z)^\dagger\mathbf{Q}_\phi^{-1}\\
&\quad\times(\boldsymbol{\phi}_z-\mathbf{r}_z+\mathbf{N}\lambda+c\boldsymbol{\delta}_z)\},
\end{aligned}\tag{9}$$

and $\boldsymbol{\Psi}_{i1}=[\Delta\psi_{i1}(t_1),\Delta\psi_{i1}(t_2),\ldots,\Delta\psi_{i1}(t_K)]$ is the $(i-1)$-th row of $\boldsymbol{\Psi}$; $\Delta\boldsymbol{\delta}_i=[\delta_{i1}(t_1)-\delta_{i1}(t_0),\delta_{i1}(t_2)-\delta_{i1}(t_0),\ldots,\delta_{i1}(t_K)-\delta_{i1}(t_0)]$ is the vector of time-differential clock offsets from time t_0 to time t; $\mathbf{r}_z=[r_{21},r_{31},\ldots,r_{M1}]^\dagger$ collects the actual distance difference between BS 1 and the other BSs; $\mathbf{D}_z=[d_{21}(\tau_z),d_{31}(\tau_z),\ldots,d_{M1}(\tau_z)]^\dagger$ is the z-th column of $\mathbf{D}$; $\boldsymbol{\phi}_z=[\phi_{21}(\tau_z),\phi_{31}(\tau_z),\ldots,\phi_{M1}(\tau_z)]^\dagger$ is the z-th column of $\boldsymbol{\phi}$; $\boldsymbol{\delta}_z=[\delta_{21}(\tau_z),\delta_{31}(\tau_z),\ldots,\delta_{M1}(\tau_z)]^\dagger$ is the vector of clock offsets between the BSs at time τ_z; and the covariance matrices of the TDoA-based and CPDoA-based distance difference measurement noises are given by

$$\begin{aligned}
\boldsymbol{Q}_{td}&=\sigma_{td}^2\begin{pmatrix}1&0.5&\cdots&0.5\\0.5&1&\cdots&0.5\\\vdots&\vdots&\ddots&\vdots\\0.5&0.5&\cdots&1\end{pmatrix};\\
\boldsymbol{Q}_{\phi}&=2\sigma_{ca}^2\begin{pmatrix}1&0.5&\cdots&0.5\\0.5&1&\cdots&0.5\\\vdots&\vdots&\ddots&\vdots\\0.5&0.5&\cdots&1\end{pmatrix}.
\end{aligned}\tag{10}$$

With consideration of practical implementation, we decouple problem (8) between the estimation of the clock offsets between the BSs (i.e., the synchronization of the BSs) and the positioning of the MS. The solution obtained by solving the decoupled subproblems can be a suboptimal solution to problem (8). Nevertheless, the decoupling is reasonable because multiple (or even many) MSs may need to be located at the same time in a system. Since the clock offsets between the BSs, $\boldsymbol{\delta}$, are included in the measurements for each MS, the joint optimization of clock offsets and positions would require the coordination with all MSs, resulting in high complexity and low scalability. By decoupling the synchronization of the BSs from the positioning of the MSs, the MSs can be located separately with improved scalability. The decoupling has been implemented in practice, e.g., [42]–[44]. As a result, problem (8) is rewritten as

$$\max_{\boldsymbol{\delta}\in\mathbb{R}} p(\mathbf{T},\boldsymbol{\Psi}|\boldsymbol{\delta})\max_{\mathbf{N}\in\mathbb{Z},\boldsymbol{\theta}\in\mathbb{R}} p(\mathbf{D},\boldsymbol{\phi}|\boldsymbol{\theta},\mathbf{N},\boldsymbol{\delta}), \tag{11}$$

where

$$\begin{aligned}
&p(\mathbf{T},\boldsymbol{\Psi}|\boldsymbol{\delta})\\
&=\prod_{i=2}^{M}\prod_{k=1}^{K}\frac{1}{\sqrt{2\pi}\sigma_{toa}}\exp\{-\frac{(T_{i1}(t_k)-d_{i1}+c\delta_{i1}(t_k))^2}{2\sigma_{toa}^2}\}\\
&\quad\times\prod_{i=2}^{M}\frac{1}{(2\pi)^{K/2}|\mathbf{Q}_\phi|^{1/2}}\\
&\quad\exp\{-\frac{1}{2}(\boldsymbol{\Psi}_{i1}+c\Delta\boldsymbol{\delta}_{i1})\mathbf{Q}_\phi^{-1}(\boldsymbol{\Psi}_{i1}+c\Delta\boldsymbol{\delta}_{i1})^\dagger\},
\end{aligned}\tag{12}$$

and

$$\begin{aligned}
&p(\mathbf{D},\boldsymbol{\phi}|\boldsymbol{\theta},\mathbf{N},\boldsymbol{\delta})\\
&=\prod_{z=1}^{Z}\frac{1}{(2\pi)^{(M-1)/2}|\mathbf{Q}_{td}|^{1/2}}\\
&\quad\exp\{-\frac{1}{2}(\mathbf{D}_z-\mathbf{r}_z+c\boldsymbol{\delta}_z)^\dagger\mathbf{Q}_{td}^{-1}(\mathbf{Q}_z-\mathbf{r}_z+c\boldsymbol{\delta}_z)\}\\
&\quad\times\prod_{z=1}^{Z}\frac{1}{(2\pi)^{(M-1)/2}|\mathbf{Q}_\phi|^{1/2}}\\
&\quad\exp\{-\frac{1}{2}(\boldsymbol{\phi}_z-\mathbf{r}_z+\mathbf{N}\lambda+c\boldsymbol{\delta}_z)^\dagger\mathbf{Q}_\phi^{-1}\\
&\quad\times(\boldsymbol{\phi}_z-\mathbf{r}_z+\mathbf{N}\lambda+c\boldsymbol{\delta}_z)\}.
\end{aligned}\tag{13}$$

Problem (11) can be solved by sequentially solving the following two subproblems: (a) a clock synchronization subproblem which estimates the clock offsets between the BSs, $\boldsymbol{\delta}$, based on the ToA- and CPoA-based distance measurements between the BSs, i.e., $\mathbf{T},\boldsymbol{\Psi}$; and (b) an integer ambiguity resolution and positioning subproblem which estimates the integer ambiguities of the carrier phase measurements, $\mathbf{N}$, and subsequently the MS position, $\boldsymbol{\theta}$, given the estimated clock offsets between the BSs, $\widehat{\boldsymbol{\delta}}$.

The clock synchronization subproblem, and the integer ambiguity resolution and positioning subproblem, are respectively given by

$$\max_{\boldsymbol{\delta}\in\mathbb{R}} p(\mathbf{T},\boldsymbol{\Psi}|\boldsymbol{\delta}), \tag{14}$$

and

$$\max_{\mathbf{N}\in\mathbb{Z},\boldsymbol{\theta}\in\mathbb{R}} p(\mathbf{D},\boldsymbol{\phi}|\boldsymbol{\theta},\mathbf{N},\widehat{\boldsymbol{\delta}}), \tag{15}$$

which are solved in Sections IV and V, respectively.

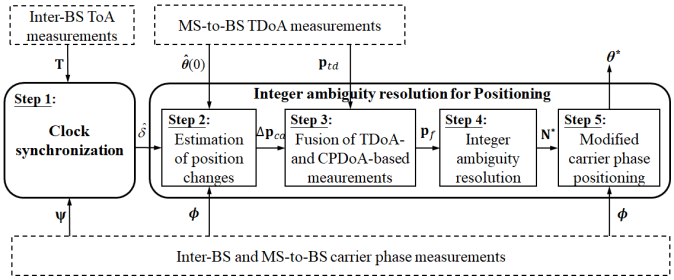

Fig. 3. The complete procedure of the proposed carrier phase positioning technique.

B. Overview of the Proposed Solution

The proposed positioning technique consists of 1) estimation of clock offsets between the BSs based on the ToA-based and CPoA-based distance measurements, 2) estimation of the MS' position changes over time based on the changes of the CPDoA-based distance difference measurements, 3) interim estimation of the MS positions by fusing the TDoA-based distance difference measurements with the estimated position changes, 4) resolution of the integer ambiguities in the CPDoA-based measurements by linearizing the measurements at the interim position estimates, and 5) refinement of the position estimations. Step 1 solves problem (14), and Steps 2 – 5 solve problem (15).

Two new techniques, namely, "Estimation of position changes" and "Fusion of TDoA- and CPDoA-based measurements", are developed in Steps 2 and 3 to help resolve the integer ambiguity of the CPDoA-based distance difference measurements. In Step 2, the position changes of the MS between any two consecutive samples are first estimated based on the initial position or its estimate $\hat{\boldsymbol{\theta}}(0)$ and the CPDoA-based distance difference measurements $\boldsymbol{\phi}$. Being insusceptible to the integer ambiguities, estimated position changes are accurate and fused with TDoA-based positioning to obtain quality interim estimation of the MS positions in Step 3. By linearizing the carrier phase measurements at the interim estimations of the MS positions, the integer ambiguities $\mathbf{N}$ can be resolved by the least-squares ambiguity decorrelation adjustment (LAMBDA) method in Step 4, and canceled to achieve accurate final estimation of the MS positions based on the disambiguated carrier phase measurements. The complete process of the proposed positioning method is illustrated in Fig. 3.

IV. ToA/CPoA-Based Clock Synchronization

By transforming (14) to a linear parameter estimation problem, a clock synchronization method is proposed based on the accumulated ToA- and CPoA-based distance measurements between the BSs, and proved to asymptotically converge to the CRLB. The relative clock offset $b_i(t)$ between BS i and the MS, i.e., (5), is time-varying [45], [46]. By utilizing the ToA-based measurement (5) alone for clock synchronization, the relative clock offset (in seconds) between the BSs is given by

$$\widetilde{\delta}_{i1}(t) = (d_{i1} - T_{i1}(t))/c. \tag{16}$$

The estimated clock offset $\widetilde{\delta}_{i1}(t)$ follows the Gaussian distribution $\mathcal{N}(\delta_{i1}(t), \sigma_{toa}^2/c^2)$, and the estimation accuracy is susceptible to the relatively large variance of the ToA-based distance measurement noise.

We propose to estimate the clock offset by incorporating the time-differential CPoA-based measurement between the BSs, $\Delta\psi_{i1}(t)$ in (7), into problem (14). As exhibited in (7), $\Delta\psi_{i1}(t)$ is approximately linear to the change of the relative clock offset between the BSs, i.e., $\delta_{i1}(t) - \delta_{i1}(t_0)$. As a result, the clock offset $\delta_{i1}(t)$ can be estimated based on $\Delta\psi_{i1}$ and $\delta_{i1}(t_0)$.

Except the reference BS, i.e., BS 1, the rest of the BSs can be independently synchronized with BS 1. Problem (14) can be decoupled between the BSs: For BS i ($i \neq 1$),

$$\max_{\boldsymbol{\delta}_{i1} \in \mathbb{R}} p(\mathbf{T}_{i1}, \boldsymbol{\Psi}_{i1} | \boldsymbol{\delta}_{i1}), \tag{17}$$

which is a linear least squares problem and can be solved by using the MLE technique.

With the probability distribution functions (PDFs) of the ToA-based measurements $\mathbf{T}_{i1} = \big[T_{i1}(t_1),\ \ldots,\ T_{i1}(t_K)\big]$ and the time-differential CPoA-based measurements $\boldsymbol{\Psi}_{i1} = [\Delta\psi_{i1}(t_1),\ \Delta\psi_{i1}(t_2), \ldots, \Delta\psi_{i1}(t_K)]$, the likelihood function of the clock offset vector $\boldsymbol{\Omega}_i = \big[\delta_{i1}(t_0), \ldots, \delta_{i1}(t_K)\big]$ can be written as

$$\begin{aligned} f(\boldsymbol{\Omega}_i) &= p(\mathbf{T}_{i1}, \boldsymbol{\Psi}_{i1} | \boldsymbol{\Omega}_i) \\ &= \prod_{k=1}^{K} \frac{1}{\sqrt{2\pi}\sigma_{toa}} \exp\{-\frac{(T_{i1}(t_k) - d_{i1} + c\delta_{i1}(t_k))^2}{2\sigma_{toa}^2}\} \\ &\quad \times \frac{1}{(2\pi)^{K/2} |\mathbf{Q}_\phi|^{1/2}} \\ &\quad \exp\{-\frac{1}{2}(\boldsymbol{\Psi}_{i1} + c\Delta\boldsymbol{\delta}_{i1}) \mathbf{Q}_\phi^{-1} (\boldsymbol{\Psi}_{i1} + c\Delta\boldsymbol{\delta}_{i1})^\dagger\}. \end{aligned} \tag{18}$$

The corresponding log-likelihood is given by

$$\begin{aligned} \mathcal{L}(\boldsymbol{\Omega}_i) = &-K\ln(2\pi) - \frac{K}{2}\ln(\sigma_{toa}^2) - \frac{1}{2}\ln(|\mathbf{Q}_\phi|) \\ &-\frac{1}{2\sigma_{toa}^2}\sum_{k=1}^{K}\Big(T_{i1}(t_k) - d_{i1} + c\delta_{i1}(t_k)\Big)^2 \\ &-\frac{1}{2}(\boldsymbol{\Psi}_{i1} + c\Delta\boldsymbol{\delta}_{i1}) \mathbf{Q}_\phi^{-1} (\boldsymbol{\Psi}_{i1} + c\Delta\boldsymbol{\delta}_{i1})^\dagger, \end{aligned} \tag{19}$$

and the maximum likelihood estimator of $\boldsymbol{\Omega}_i$ is given by

$$\hat{\boldsymbol{\Omega}}_i = \arg\max_{\hat{\boldsymbol{\Omega}}_i} \mathcal{L}(\hat{\boldsymbol{\Omega}}_i). \tag{20}$$

Given the continuity and differentiability of (19), the maximum likelihood estimator yields

$$\begin{aligned} &\frac{\partial\mathcal{L}(\boldsymbol{\Omega}_i)}{\partial\delta_{i1}(t_k)} \\ &= -\frac{c\Big(T_{i1}(t_k) - d_{i1} + c\delta_{i1}(t_k)\Big)}{\sigma_{toa}^2} \\ &\quad -\frac{c}{\sigma_{ca}^2}\Big(\psi_{i1}(t_k) - \psi_{i1}(t_0) + c\delta_{i1}(t_k) - c\delta_{i1}(t_0))\Big) \\ &\quad +\frac{c}{(K+1)\sigma_{ca}^2}\sum_{t=t_1}^{t_K}\Big(\psi_{i1}(t) - \psi_{i1}(t_0) + c\delta_{i1}(t) - c\delta_{i1}(t_0))\Big), \end{aligned} \tag{21}$$

$$\frac{\partial \mathcal{L}(\mathbf{\Omega}_i)}{\partial \delta_{i1}(t_0)} = \frac{c}{(K+1)\sigma_{ca}^2} \sum_{t=t_1}^{t_K} \Big(\psi_{i1}(t) - \psi_{i1}(t_0) + c\delta_{i1}(t) - c\delta_{i1}(t_0) \Big). \tag{22}$$

By setting both (21) and (22) to 0 and jointly solving them, $\delta_{i1}(t_0)$ can be estimated as

$$\hat{\delta}_{i1}(t_0) = \frac{1}{cK} \sum_{t=t_1}^{t_K} \Big(d_{i1} - T_{i1}(t) - \psi_{i1}(t_0) + \psi_{i1}(t) \Big), \tag{23}$$

which follows the Gaussian distribution $\mathcal{N}(\delta_{i1}(t_0), \frac{\sigma_{toa}^2}{c^2 K} + \frac{(K+1)\sigma_{ca}^2}{c^2 K})$.

Finally, the clock offset between BSs i and 1 at any time t is estimated as

$$\hat{\delta}_{i1}(t) = \hat{\delta}_{i1}(t_0) + (\psi_{i1}(t_0) - \psi_{i1}(t))/c, \tag{24}$$

which follows the Gaussian distribution $\mathcal{N}(\delta_{i1}(t), \frac{\sigma_{toa}^2}{c^2 K} + \frac{(K-1)\sigma_{ca}^2}{c^2 K})$. (24) is the unbiased estimator of $\delta_{i1}(t)$, and the variance can be reduced by increasing measurements.

To evaluate the accuracy of (24), we analyze the CRLB which provides the minimum variance of estimation [47]. Based on (19), the Fisher information matrix (FIM) of $\mathbf{\Omega}_i$ is given by [48]

$$J(\hat{\mathbf{\Omega}}_i) = \begin{pmatrix} -\mathbb{E}[\frac{\partial^2 \mathcal{L}(\mathbf{\Omega}_i)}{\partial \delta_{i1}^2(t_0)}] & \cdots & -\mathbb{E}[\frac{\partial^2 \mathcal{L}(\mathbf{\Omega}_i)}{\partial \delta_{i1}(t_0) \partial \delta_{i1}(t_K)}] \\ \vdots & \ddots & \vdots \\ -\mathbb{E}[\frac{\partial^2 \mathcal{L}(\mathbf{\Omega}_i)}{\partial \delta_{i1}(t_K) \partial \delta_{i1}(t_0)}] & \cdots & -\mathbb{E}[\frac{\partial^2 \mathcal{L}(\mathbf{\Omega}_i)}{\partial \delta_{i1}^2(t_K)}] \end{pmatrix}. \tag{25}$$

By taking the second derivatives of (21) and (22) and then expectations over $T_{i1}(t)$ and $\psi_{i1}(t)$, the (m,n)-th entry of the FIM is given by

$$\Big(J(\hat{\mathbf{\Omega}}_i)\Big)_{m,n} = \begin{cases} -\mathbb{E}[\frac{\partial^2 \mathcal{L}(\mathbf{\Omega}_i)}{\partial \delta_{i1}^2(t_0)}] = \frac{K}{K+1}\frac{c^2}{\sigma_{ca}^2}, \\ \qquad \text{if } m=1, n=1; \\ -\mathbb{E}[\frac{\partial^2 \mathcal{L}(\mathbf{\Omega}_i)}{\partial \delta_{i1}^2(t_{m-1})}] = \frac{(K+1)\sigma_{ca}^2 + K\sigma_{toa}^2}{(K+1)\sigma_{ca}^2\sigma_{toa}^2} c^2, \\ \qquad \text{if } m=n\neq 1; \\ -\mathbb{E}[\frac{\partial^2 \mathcal{L}(\mathbf{\Omega}_i)}{\partial \delta_{i1}(t_{m-1}) \partial \delta_{i1}(t_{n-1})}] = -\frac{1}{K+1}\frac{c^2}{\sigma_{ca}^2}, \\ \qquad \text{otherwise.} \end{cases} \tag{26}$$

We note that the second derivatives are independent of $T_{i1}(t)$ and $\psi_{i1}(t)$, and therefore equal to their expectations over $T_{i1}(t)$ and $\psi_{i1}(t)$. Then, the (m,n)-th entry of the inverse of the FIM is given by

$$\Big(J^{-1}(\hat{\mathbf{\Omega}}_i)\Big)_{m,n} = \begin{cases} \frac{(K+1)\sigma_{ca}^2 + \sigma_{toa}^2}{Kc^2}, & \text{if } m=1, n=1; \\ \frac{\sigma_{toa}^2}{Kc^2}, & \text{if } m=1, n>1; \\ \frac{\sigma_{toa}^2}{Kc^2}, & \text{if } m>1, n=1; \\ \frac{\sigma_{ca}^2\sigma_{toa}^2}{(\sigma_{ca}^2+\sigma_{toa}^2)c^2} + \frac{\sigma_{toa}^4}{K(\sigma_{ca}^2+\sigma_{toa}^2)c^2}, & \text{if } m=n\neq 1; \\ \frac{\sigma_{toa}^4}{K(\sigma_{ca}^2+\sigma_{toa}^2)c^2}, & \text{otherwise.} \end{cases} \tag{27}$$

According to the CRLB inequality [46], the lower bound of the clock offset estimation variance is given by

$$CRLB(\delta_{i1}(t_K)) \geq \Big(J(\hat{\mathbf{\Omega}}_i)^{-1}\Big)_{K+1,K+1} = \frac{\sigma_{ca}^2\sigma_{toa}^2}{(\sigma_{ca}^2+\sigma_{toa}^2)c^2} + \frac{\sigma_{toa}^4}{K(\sigma_{ca}^2+\sigma_{toa}^2)c^2}. \tag{28}$$

Given $\sigma_{ca} \ll \sigma_{toa}$, we can show that the estimation variance of (24) can asymptotically and indistinguishably converge to the CRLB (28) with the increasing number of samples, i.e.,

$$\lim_{K\to+\infty} \left[\left(\frac{\sigma_{toa}^2}{c^2 K} + \frac{(K-1)\sigma_{ca}^2}{c^2 K} \right) - \left(\frac{\sigma_{ca}^2\sigma_{toa}^2}{(\sigma_{ca}^2+\sigma_{toa}^2)c^2} + \frac{\sigma_{toa}^4}{K(\sigma_{ca}^2+\sigma_{toa}^2)c^2} \right) \right] = \frac{\sigma_{ca}^4}{(\sigma_{ca}^2+\sigma_{toa}^2)c^2} \to 0. \tag{29}$$

The high-accuracy clock offset estimation allows the difference between the joint optimization problem (8) and the subproblems to diminish, with the increasing number of measurements.

V. Integer Ambiguity Resolution and Carrier Phase Positioning

In this section, we solve the integer ambiguity resolution and positioning subproblem, i.e., problem (15), which is an NP-hard NMIP. The problem is solved by first estimating the MS position changes accurately based on the temporal changes of the CPDoA-based distance difference measurements, and fusing the position changes with TDoA-based positioning results. In this way, we circumvent the integer ambiguities of the CPDoA-based measurements and obtain quality interim estimates of the MS positions, at which the CPoA-based distance measurements (3) can be linearized to transform problem (15) to a linear mixed-integer program and resolve the integer ambiguities. The precise MS positions can be obtained based on the disambiguated CPDoA-based measurements. The details are following.

A. Estimation of Position Changes

We start with the new algorithm to estimate the position changes of the MS between two consecutive samples by using the ambiguous CPDoA-based measurements, as given in (4). As mentioned in Section II, the integer ambiguity of a link from the MS to a BS remains unchanged if the PLL keeps locking the carrier phase. For this reason, the integer ambiguity is suppressed by measuring the temporal change of

the CPDoA-based distance difference measurements between two consecutive samples. The temporal change corresponds to the "double-differential carrier phase measurement" in the context of GPS/GNSS [22].

Based on (4), the unambiguous temporal change of the CPDoA-based distance difference measurements is given by

$$\Delta\phi_{i1}(t) = r_{i1}(t) - r_{i1}(t-1) - c\Delta\delta_{i1}(t) + \Delta n_{i1}^{ca}(t), \quad (30)$$

where $\Delta n_{i1}^{ca}(t) = n_{i1}^{ca}(t) - n_{i1}^{ca}(t-1)$, and $\Delta\delta_{i1}(t) = \delta_{i1}(t) - \delta_{i1}(t-1)$ which only involves the clock offset between BSs i and 1.

Since $\Delta n_{i1}^{ca}(t)$ is a zero-mean Gaussion noise and $\hat{\delta}_{i1}(t)$ is the unbiased estimator of $\delta_{i1}(t)$, $\Delta\phi_{i1}(t) + c\Delta\hat{\delta}_{i1}(t)$ is the unbiased estimator of $r_{i1}(t) - r_{i1}(t-1)$. We move $r_i(t)$ from the right-hand side of (30) to the left-hand side, next move other terms to the right-hand side, then take squares on both sides, and finally rewrite (30) as

$$-2\boldsymbol{\zeta}_{i1}^{\dagger}\boldsymbol{\theta}(t) - 2U_{i1}(t)r_1(t) = U_{i1}^2(t) - K_{i1}, \quad (31)$$

where $\boldsymbol{\zeta}_{i1}^{\dagger} = \boldsymbol{\zeta}_i^{\dagger} - \boldsymbol{\zeta}_1^{\dagger}$, $U_{i1}(t) = \Delta\phi_{i1}(t) + c\Delta\hat{\delta}_{i1}(t) + r_{i1}(t-1) - \Delta n_{i1}^{ca}(t)$, and $K_{i1} = \boldsymbol{\zeta}_i^{\dagger}\boldsymbol{\zeta}_i - \boldsymbol{\zeta}_1^{\dagger}\boldsymbol{\zeta}_1$ for notational simplicity.

For $i = 2, 3, \cdots, M$, (31) can be collectively rewritten in the format of matrix, as given by

$$\mathbf{G}(t)\mathbf{z}(t) = \mathbf{h}(t), \quad (32)$$

where

$$\mathbf{G}(t) = \begin{pmatrix} -2\boldsymbol{\zeta}_{21}^T & -2U_{21}(t) \\ -2\boldsymbol{\zeta}_{31}^T & -2U_{21}(t) \\ \vdots & \vdots \\ -2\boldsymbol{\zeta}_{M1}^T & -2U_{M1}(t) \end{pmatrix}, \quad \mathbf{z}(t) = \begin{pmatrix} \boldsymbol{\theta}(t) \\ r_1(t) \end{pmatrix},$$

$$\mathbf{h}(t) = \begin{pmatrix} U_{21}^2(t) - K_{21} \\ U_{31}^2(t) - K_{31} \\ \vdots \\ U_{M1}^2(t) - K_{M1} \end{pmatrix}.$$

In (32), there are only two unknown position variables $\boldsymbol{\theta}(t-1)$ and $\boldsymbol{\theta}(t)$, which are part of $U_{i1}(t)$ and $z(t)$, respectively.

Suppose that the positioning process starts at time $t = 0$ with the estimated initial position of the MS, $\hat{\boldsymbol{\theta}}(0) = \big[x(0), y(0), z(0)\big]^{\dagger}$. By taking the previous estimation $\hat{\boldsymbol{\theta}}(t-1)$ as a known parameter, the MS position $\boldsymbol{\theta}(t)$ in (32) can be estimated using Chan's method [9]. Therefore, $\boldsymbol{\theta}$ can be estimated iteratively over time. We denote the estimation at time t by $\mathbf{p}_{ca}(t) = \hat{\boldsymbol{\theta}}(t)$. The initial position $\hat{\boldsymbol{\theta}}(0)$ can be estimated by the classical TDoA-based positioning method [9], i.e., $\mathbf{p}_{ca}(0) = \hat{\boldsymbol{\theta}}(0)$. The position change of the MS is given by

$$\Delta\mathbf{p}_{ca}(t) = \mathbf{p}_{ca}(t) - \mathbf{p}_{ca}(t-1). \quad (33)$$

While the accuracy of $\mathbf{p}_{ca}(t)$ depends primarily on the TDoA-based estimation of the initial position which can have a large variance, the position changes in (33) are estimated from unambiguous temporal changes of the CPDoA-based measurements, and therefore accurate.

B. Fusion of TDoA-and CPDoA-Based Measurements

We propose to fuse the accurate estimations of the position changes, $\Delta\mathbf{p}_{ca}(t)$, and the TDoA-based positioning results, $\mathbf{p}_{td}(t)$, to obtain the quality interim estimations of the MS positions $\mathbf{p}_f(t)$. The estimation process of $\mathbf{p}_f(t)$ is given in Algorithm 1. We note that Kalman filter can perform state estimation based on the current measurements and the previous estimation. A motion model (e.g., based on speed and acceleration) is often needed for the state estimation in Kalman filter, and the covariance of the process noise accounting for the motion model error is needed in prior to adjust the Kalman gain [49], [50]. In contrast, Algorithm 1 does not assume any motion model, and therefore is resistant to inexact a-priori knowledge of the process noise.

Algorithm 1 Fusion-Based Estimation Using TDoA- and CPDoA-Based Measurements

Require: Estimated positions $\mathbf{p}_{td}(t)$ and $\mathbf{p}_{ca}(t)$ obtained by TDoA- and ambiguous CPDoA-based measurements

Ensure: Interim estimations of positions $\mathbf{p}_f(t)$

1: $\mathbf{p}_f(0) = \mathbf{p}_{td}(0)$; $\mathbf{p}_{ca}(0) = \mathbf{p}_{td}(0)$
   % Set the initial point of the fusion-based estimation using the TDoA-based distance difference measurements
2: **for** $t = 1$ to T_{end} **do**
3: $\Delta\mathbf{p}_{ca}(t) = \mathbf{p}_{ca}(t) - \mathbf{p}_{ca}(t-1)$
   % Estimate the position change based on the temporal changes of the CPDoA-based distance difference measurements
4: $\widetilde{\mathbf{p}}_{ca}(t) = \mathbf{p}_f(t-1) + \Delta\mathbf{p}_{ca}(t)$
   % Update the position estimation with the estimated position change
5: $\mathbf{p}_f(t) = w_{td}\mathbf{p}_{td}(t) + w_{ca}\widetilde{\mathbf{p}}_{ca}(t)$
   % Fuse the position estimates
6: **end for**

The estimation of $\mathbf{p}_f(t)$ is initialized with the TDoA-based estimation of the initial MS position, i.e., $\mathbf{p}_f(0) = \mathbf{p}_{td}(0)$. The estimation variance of $\mathbf{p}_{td}(0)$ is linear to σ_{td}^2, i.e., $\mathrm{Var}(\mathbf{p}_{td}(0)) \propto \sigma_{td}^2$, where $\mathrm{Var}(X)$ stands for the variance of X, and "$\propto$" stands for "is proportional to". At each time t, we first estimate the position change $\Delta\mathbf{p}_{ca}(t)$ according to (33), and the estimation variance of $\Delta\mathbf{p}_{ca}(t)$ follows

$$\mathrm{Var}(\Delta\mathbf{p}_{ca}(t)) \propto 2\sigma_{ca}^2. \quad (34)$$

Given the fine accuracy of $\Delta\mathbf{p}_{ca}(t)$, we update the position estimation $\widetilde{\mathbf{p}}_{ca}(t) = \mathbf{p}_f(t-1) + \Delta\mathbf{p}_{ca}(t)$, whose estimation variance is given by

$$\mathrm{Var}(\widetilde{\mathbf{p}}_{ca}(t)) = \mathrm{Var}(\mathbf{p}_f(t-1)) + \mathrm{Var}(\Delta\mathbf{p}_{ca}(t)). \quad (35)$$

Unbiased estimation of the MS positions can also be obtained with the TDoA-based measurements at time t. As shown in Algorithm 1, the unbiased estimate $\mathbf{p}_{td}(t)$ is further fused through $\mathbf{p}_f(t) = w_{td}\mathbf{p}_{td}(t) + w_{ca}\widetilde{\mathbf{p}}_{ca}(t)$ with non-negative weighting coefficients w_{td} and w_{ca}, where $w_{td} + w_{ca} = 1$ and

$$\mathrm{Var}(\mathbf{p}_f(t)) = w_{td}^2\mathrm{Var}(\mathbf{p}_{td}(t)) + w_{ca}^2\mathrm{Var}(\widetilde{\mathbf{p}}_{ca}(t)). \quad (36)$$

From (35) and (36), the estimation variance of $\mathbf{p}_f$ is given by

$$\begin{aligned}\mathrm{Var}(\mathbf{p}_f(t)) &\propto \left(w_{td}^2\sum_{i=1}^{t} w_{ca}^{2(i-1)} + w_{ca}^{2t}\right)\sigma_{td}^2 + 2\sum_{i=1}^{t} w_{ca}^{2i}\sigma_{ca}^2 \\ &= \left(w_{td}^2\frac{1-w_{ca}^{2t}}{1-w_{ca}^2} + w_{ca}^{2t}\right)\sigma_{td}^2 + 2w_{ca}^2\frac{1-w_{ca}^{2t}}{1-w_{ca}^2}\sigma_{ca}^2. \end{aligned} \tag{37}$$

The convergence of Algorithm 1 is confirmed by evaluating the variation of (37). In particular,

$$\begin{aligned}&\mathrm{Var}(\mathbf{p}_f(t)) - \mathrm{Var}(\mathbf{p}_f(t-1)) \\ &\quad\propto w_{ca}^{2(t-1)}\left((w_{td}^2 + w_{ca}^2 - 1)\sigma_{td}^2 + 2w_{ca}^2\sigma_{ca}^2\right) \\ &\quad= 2w_{ca}^{2t-1}\left((1-w_{td})\sigma_{ca}^2 - w_{td}\sigma_{td}^2\right). \end{aligned} \tag{38}$$

If $w_{td} > \frac{\sigma_{ca}^2}{\sigma_{ca}^2+\sigma_{td}^2}$, the estimation variance of $\mathbf{p}_f(t)$ decreases monotonically over time. Additionally, since $0 < w_{ca} < 1$, the estimation variance of $\mathbf{p}_f(t)$ diminishes, as given by

$$\begin{aligned}&\lim_{t\to\infty}\left(\mathrm{Var}(\mathbf{p}_f(t)) - \mathrm{Var}(\mathbf{p}_f(t-1))\right) \\ &\qquad\propto \lim_{t\to\infty}\left(2w_{ca}^{2t-1}\left((1-w_{td})\sigma_{ca}^2 - w_{td}\sigma_{td}^2\right)\right) = 0, \end{aligned} \tag{39}$$

which converges to

$$\begin{aligned}&\lim_{t\to\infty}\mathrm{Var}(\mathbf{p}_f(t)) \\ &\quad\propto \lim_{t\to\infty}\left((w_{td}^2\frac{1-w_{ca}^{2t}}{1-w_{ca}^2} + w_{ca}^{2t})\sigma_{td}^2 + 2w_{ca}^2\frac{1-w_{ca}^{2t}}{1-w_{ca}^2}\sigma_{ca}^2\right) \\ &\quad= \frac{w_{td}^2}{1-w_{ca}^2}\sigma_{td}^2 + 2\frac{w_{ca}^2}{1-w_{ca}^2}\sigma_{ca}^2. \end{aligned} \tag{40}$$

The estimated MS positions of Algorithm 1 are more accurate than $\mathbf{p}_{ca}(t)$ if the weighting coefficients are carefully selected based on (40). Despite circumventing the integer ambiguities of the CPDoA-based distance difference measurements (by only using the position changes), the accuracy of $\mathbf{p}_f(t)$ still heavily relies on the TDoA-based distance measurements which suffer from large variances.

C. Integer Ambiguity Resolution

Given the quality interim estimation of the MS positions obtained in Algorithm 1, we can resolve the integer ambiguities of the CPDoA-based distance difference measurements by linearizing the CPoA-based distance measurements at the interim estimation. After resolving the integer ambiguities, we use the unambiguous CPDoA-based measurements for high-accuracy positioning.

1) Linearization of Integer Ambiguity: Given the quality interim estimation of the MS positions $\mathbf{p}_f(t) = (x(t), y(t), z(t))$, $\forall t$, we can effectively linearize (3) with the Taylor series expansion. With the second- or higher-order terms suppressed, (3) can be transformed into

$$\begin{aligned}&\phi_i(t) - \rho_i(t) + cb_i(t) \\ &\qquad= [\alpha_i(t), \beta_i(t), \gamma_i(t)]\boldsymbol{\theta}(t) - \lambda N_i + n_i^{ca}(t), \end{aligned} \tag{41}$$

where $\rho_i(t) = \frac{\boldsymbol{\zeta}_i^T\boldsymbol{\zeta}_i - \boldsymbol{\zeta}_i\mathbf{p}_f(t)}{\|\boldsymbol{\zeta}_i - \mathbf{p}_f(t)\|_2}$, $\alpha_i(t) = \frac{x_f(t)-A_i}{\|\boldsymbol{\zeta}_i - \mathbf{p}_f(t)\|_2}$, $\beta_i(t) = \frac{y_f(t)-B_i}{\|\boldsymbol{\zeta}_i - \mathbf{p}_f(t)\|_2}$, and $\gamma_i(t) = \frac{z_f(t)-C_i}{\|\boldsymbol{\zeta}_i - \mathbf{p}_f(t)\|_2}$.

By evaluating the difference of (41) between BSs i and 1, we obtain

$$\varphi_{i1}(t) = [\alpha_{i1}(t), \beta_{i1}(t), \gamma_{i1}(t)]\boldsymbol{\theta}(t) - \lambda N_{i1} + n_{i1}^{ca}(t), \tag{42}$$

where $\varphi_{i1}(t) = \phi_{i1}(t) - \rho_{i1}(t) + cb_{i1}(t)$ and $\varphi_{i1}(t)$ can be substituted by $\phi_{i1}(t) - \rho_{i1}(t) + c\hat{\delta}_{i1}(t)$.

For $i = 2, 3, \cdots, M$, (42) can be rewritten in the form of matrix, as given by

$$\boldsymbol{\varphi}(t) = \mathbf{H}(t)\boldsymbol{\theta}(t) - \lambda\mathbf{N} + \mathbf{n}(t), \tag{43}$$

where

$$\boldsymbol{\varphi}(t) = \begin{pmatrix}\varphi_{21}(t)\\ \varphi_{31}(t)\\ \vdots\\ \varphi_{M1}(t)\end{pmatrix}, \quad \mathbf{H}(t) = \begin{pmatrix}\alpha_{21}(t) & \beta_{21}(t) & \gamma_{21}(t)\\ \vdots & \vdots & \vdots\\ \alpha_{M1}(t) & \beta_{M1}(t) & \gamma_{M1}(t)\end{pmatrix},$$

$$\mathbf{N} = \begin{pmatrix}N_{21}\\ N_{31}\\ \vdots\\ N_{M1}\end{pmatrix},$$

and

$$\mathbf{n}(t) = \begin{pmatrix}n_{21}^{ca}(t)\\ n_{31}^{ca}(t)\\ \vdots\\ n_{M1}^{ca}(t)\end{pmatrix}.$$

Clearly, (43) is linear to the position variable $\boldsymbol{\theta}(t)$, and the integer ambiguity variable $\mathbf{N}$.

By stacking the CPDoA-based measurements from time $t = \tau_1$ to $t = \tau_Z$, (43) becomes

$$\boldsymbol{\varphi} = \mathbf{H}\boldsymbol{\xi} + \mathbf{n}, \tag{44}$$

where

$$\boldsymbol{\varphi} = \begin{pmatrix}\boldsymbol{\varphi}(1)\\ \boldsymbol{\varphi}(2)\\ \vdots\\ \boldsymbol{\varphi}(Z)\end{pmatrix}, \quad \mathbf{H} = \begin{pmatrix}\mathbf{H}(1) & \cdots & \mathbf{0} & -\lambda\mathbf{I}_{(M-1)}\\ \vdots & \ddots & \vdots & \vdots\\ \mathbf{0} & \cdots & \mathbf{H}(Z) & -\lambda\mathbf{I}_{(M-1)}\end{pmatrix},$$

$$\boldsymbol{\xi} = \begin{pmatrix}\boldsymbol{\theta}(1)\\ \boldsymbol{\theta}(2)\\ \vdots\\ \boldsymbol{\theta}(Z)\\ \mathbf{N}\end{pmatrix}, \quad \mathbf{n} = \begin{pmatrix}\mathbf{n}(1)\\ \mathbf{n}(2)\\ \vdots\\ \mathbf{n}(Z)\end{pmatrix},$$

and $\mathbf{I}_{(M-1)}$ is the $(M-1)\times(M-1)$ identity matrix. The covariance matrix of the noise vector $\mathbf{n}$ is given by

$$\mathbf{Q}_\varphi = \mathbb{E}(\mathbf{n}\mathbf{n}^\dagger) = 2\sigma_{ca}^2\begin{pmatrix}1 & 0.5 & \cdots & 0.5\\ 0.5 & 1 & \cdots & 0.5\\ \vdots & \vdots & \ddots & \vdots\\ 0.5 & 0.5 & \cdots & 1\end{pmatrix}, \tag{45}$$

where $2\sigma_{ca}^2$ is the variance of the CPDoA-based distance difference measurement noise, and the off-diagonal entries 0.5 in the coefficient matrix are due to the cross-correlation between different CPDoA measurements (with the same reference BS, i.e., BS 1).

To improve tractability, we first relax $\mathbf{N} \in \mathbb{Z}^{(M-1)}$ to $\tilde{\mathbf{N}} \in \mathbb{R}^{(M-1)}$. By using the least squares error (LSE) method, we obtain

$$\tilde{\boldsymbol{\xi}} = (\mathbf{H}^T \mathbf{Q}_{\varphi}^{-1} \mathbf{H})^{-1} \mathbf{H}^{\dagger} \mathbf{Q}_{\varphi}^{-1} \boldsymbol{\varphi}, \tag{46}$$

of which the last $(M-1)$ elements provide the continuous solution to $\tilde{\mathbf{N}} \in \mathbb{R}^{(M-1)}$, i.e.,

$$\tilde{\mathbf{N}} = [\tilde{\boldsymbol{\xi}}]_{(3Z+1):(3Z+M-1)}. \tag{47}$$

We proceed to search for the integer solution to $\mathbf{N} \in \mathbb{Z}^{(M-1)}$. Based on the LSE method, the covariance of variable $\tilde{\boldsymbol{\xi}}$ is given by

$$\mathbf{Q}_{\tilde{\xi}} = (\mathbf{H}^T \mathbf{Q}_{\varphi}^{-1} \mathbf{H})^{-1}. \tag{48}$$

Since $\boldsymbol{\xi} = (\boldsymbol{\eta}, \mathbf{N})^{\dagger}$ with $\boldsymbol{\eta} = \boldsymbol{\theta}(1)^{\dagger}, \boldsymbol{\theta}(2)^{\dagger}, \cdots, \boldsymbol{\theta}(Z)^{\dagger}$, the covariance matrix can also be written as

$$\mathbf{Q}_{\tilde{\xi}} = \begin{pmatrix} \mathbf{Q}_{\boldsymbol{\eta}\boldsymbol{\zeta}} & \mathbf{Q}_{\boldsymbol{\eta}\tilde{\mathbf{N}}} \\ \mathbf{Q}_{\tilde{\mathbf{N}}\boldsymbol{\zeta}} & \mathbf{Q}_{\tilde{\mathbf{N}}\tilde{\mathbf{N}}} \end{pmatrix}, \tag{49}$$

where $\mathbf{Q}_{\boldsymbol{\eta}\boldsymbol{\eta}}$ is the $3Z \times 3Z$ matrix, and $\mathbf{Q}_{\tilde{\mathbf{N}}\tilde{\mathbf{N}}}$ is the $(M-1) \times (M-1)$ matrix. Therefore, the covariance of the continuous solution $\tilde{\mathbf{N}}$ is given by

$$\mathbf{Q}_{\tilde{\mathbf{N}}\tilde{\mathbf{N}}} = \left[\mathbf{Q}_{\tilde{\xi}}\right]_{\left((3Z+1):(3Z+M-1),(3Z+1):(3Z+M-1)\right)}. \tag{50}$$

The estimation of $\mathbf{N}$ is equivalent to the following LSE problem [51], [52].

$$\mathbf{N}^* = \underset{\mathbf{N} \in \mathbb{Z}^{M-1}}{\arg\min} (\mathbf{N} - \tilde{\mathbf{N}})^{\dagger} \mathbf{Q}_{\tilde{\mathbf{N}}\tilde{\mathbf{N}}} (\mathbf{N} - \tilde{\mathbf{N}}), \tag{51}$$

which can be efficiently solved using the classical LAMBDA method via decorrelation-based space search [52], [53].

2) Carrier Phase Positioning: With the estimated integer ambiguities $\mathbf{N}^*$, we can disambiguate the CPDoA-based distance difference measurement $\boldsymbol{\phi}(t)$ and input into the classical range-based positioning algorithm developed originally for hyperbolic positioning in [9]. The result, denoted by $\boldsymbol{\theta}^*(t)$, is the estimated MS position at time t by carrier phase positioning.

D. Consideration of Cycle Slips

A cycle slip may occur in the presence of severe multipath/NLOS. Our proposed framework can deal with cycle slips by incorporating existing cycle slip detection and compensation methods [54]–[58]. As shown in Fig. 3, in Step 1, the clock offsets between BSs are estimated based on the ToA- and CPoA-based distance measurements over a period of time, during which cycle slips can be detected and corrected by detecting the jumps in the high-order differences of the CPoA-based distance measurements. Specifically, we can detect cycle slips, including the size of cycle slips, by using high-order difference methods [58], e.g., fourth-order difference, and correct the cycle slips before estimating the clock offsets.

In Step 2, the estimation of the MS position changes only depends on the temporal changes of the CPDoA-based measurements between consecutive samples. By using the temporal changes of the measurements, the integer ambiguities are canceled in the estimation of the position changes. The step is insusceptible to the integer ambiguities and hence tolerates cycle slips. Step 3 is also insusceptible to cycle slips, given its use of only TDoA-based measurements and estimated position changes. Nevertheless, by taking fourth-order difference of the CPoA-based measurements, we can detect cycle slips (and their sizes) and correct them [58] in Step 2 in the same way as done in Step 1. With the cycle slips detected and corrected in Step 2, linearization is done in the same way as it is in the absence of cycle slips in Step 4, and so is the positioning in Step 5.

E. Complexity Analysis

The complexity of the proposed algorithm is polynomial, i.e., $\mathcal{O}\big(K(M-1) + Z(M-1)^2 + Z(M-1)^3 + Z^3(M-1)^2 (3Z + M - 1)\big)$, where $\mathcal{O}\big(K(M-1)\big)$, $\mathcal{O}\big(Z(M-1)^2\big)$, and $\mathcal{O}\big(Z(M-1)^3 + Z^3(M-1)^2 (3Z+M-1)\big)$ are the complexities of the clock offset estimation, the position estimation using Chan's method [8], [9], and the integer ambiguity resolution based on float resolution and LAMBDA method [50]–[52], respectively. Recall that Z and K are the numbers of measurements that can be used for positioning and clock offset estimation, respectively, and M is the number of BSs. On the other hand, the original problem (8) is an NMIP problem, which can be solved optimally using the branch and bound (B&B) method if solved jointly. The worst-case complexity of the B&B method is an exponential complexity and close to that of the exhaustive search, i.e., $\mathcal{O}\big((A/P_1^3)^Z (B/\lambda)^{M-1} (C/P_2)^{K(M-1)}\big)$, where $\mathcal{O}\left((A/P_1^3)^Z\right)$, $\mathcal{O}\left((B/\lambda)^{M-1}\right)$ and $\mathcal{O}\left((C/P_2)^{K(M-1)}\right)$ are the complexities of searching the time offsets, integer ambiguities, and positions, respectively. A, B, and C depend on the search spaces of the positioning space, the maximum length from one location to another within the positioning space, and the maximum clock offset, respectively. P_1 and P_2 are the desired positioning accuracy and clock offset estimation accuracy, respectively. By decoupling the original problem (as done in the proposed algorithm), the complexity of solving problem (8) is dramatically reduced, as compared to the joint estimation method.

VI. Simulation Results and Analysis

In this section, we evaluate the performance of the proposed carrier phase positioning method in wireless cellular networks. Simulations are carried out under the indoor office scenario specified in the 3GPP standard [38]. We consider the C-PRS as the reference signal for carrier phase positioning [37], and the center frequency of the C-PRS is 30 GHz, i.e., the carrier wavelength is 0.01 m. As suggested in [38, Tab. 8.1.1.6], we consider 6 BSs in the simulation. We also set the interval between two consecutive measurement reports to 100 milliseconds [59]–[61], and the number of measurements used to resolve the integer ambiguity to 50 [61]. Each simulation result is the average of 2,000 independent tests upon an MS. Since the velocity of an MS is typically up to 3 km/h in indoor environments [38], the simulated MS takes a random walk with the speed randomly and uniformly selected from $[0, 3]$ km/h in each of the tests.

It is reported in [41] and [62] that the PLL tracking error of carrier phase is about 10% of a wavelength resulting from multipath/NLoS, as compared to 1% of the wavelength

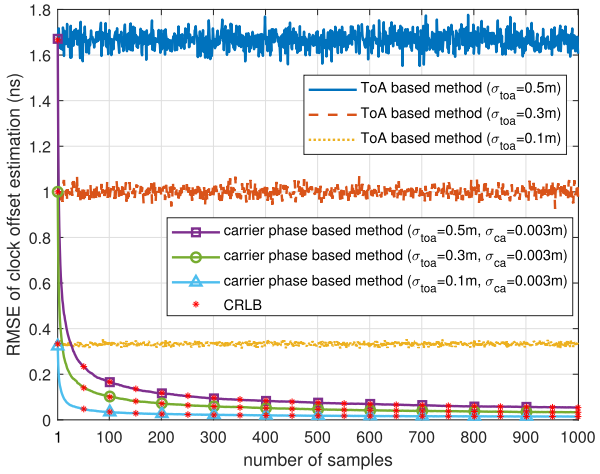

Fig. 4. Comparison of the existing ToA-based and the proposed CPoA-based clock offset estimations in the absence of cycle slips.

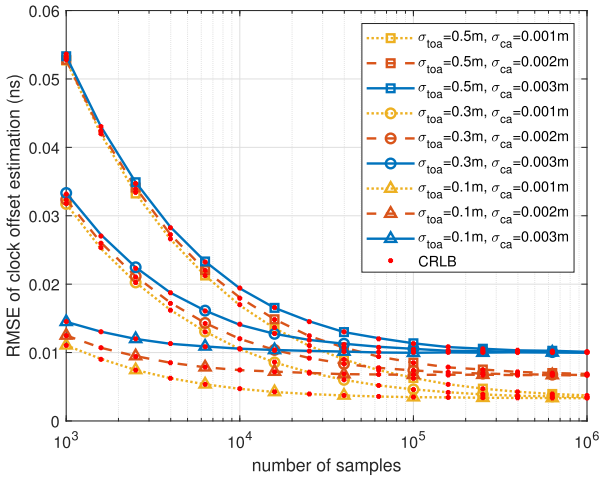

Fig. 5. Clock offset estimation performance of the proposed CPoA-based method under different STDs of the ToA-and CPoA-based distance measurements in the absence of cycle slips.

in the presence of a dominating LoS path. On the other hand, the time-delay estimation errors attributed to multipath propagations range from 0.1ns to 1ns (or equivalently, 0.03m to 0.3m in distance) in 5G systems, when the transmitter and receivers are synchronized [18], [45], [63], [64]. For this reason, we set the standard deviations (STDs) of the ToA-based distance measurement noise to 0.1m, 0.3m and 0.5m; and set the STDs of the CPoA-based distance measurement noise to 0.001m, 0.002m and 0.003m, which are 10%, 20% and 30% of a wavelength (i.e., 0.01m), respectively. We also evaluate the performance of our proposed algorithm in the presence of cycle slips. With reference to [54]–[57], we assume that the occurrences of the cycle slips follow a Poison distribution with an average interval of 10 to 100 seconds. The size of a cycle slip is randomly and uniformly distributed between -20 and 20 cycles. The fourth-order difference method [58] is applied to detect the cycle slips and their sizes. An ablation study is carried out to evaluate every step of the proposed approach in the following.

A. Performance of CPoA-Based Clock Offset Estimation

We first compare the proposed CPoA-based clock synchronization method to the ToA-based method, i.e., (16), in the absence of cycle slips. Fig. 4 shows the Root Mean Square Error (RMSE) of the clock offset estimation under different number of samples. Since the ToA-based method only utilizes the current ToA-based distance measurement to estimate the time-varying clock offset, the RMSE of the estimation is σ_{toa}/c. We see that the RMSE of the ToA-based method remains high and does not improve with the increasing number of samples. The proposed method performs much better due to the utilization of high-accuracy carrier phase measurements. With the increasing number of samples, the estimation variance of the clock offset, i.e., (24), continuously decreases. At time t_0, there are no enough carrier phase measurements to evaluate the time-differential CPoA-based distance measurement, i.e., $\Delta\psi_{i1}(t) = \psi_{i1}(t) - \psi_{i1}(t_0)$, and only a ToA-based measurement can be used for the clock offset estimation. Therefore, the RMSE is σ_{toa}/c at time t_0. The clock synchronization accuracy can be as accurate as a picosecond level, which is nearly a thousand times better than the ToA-based method.

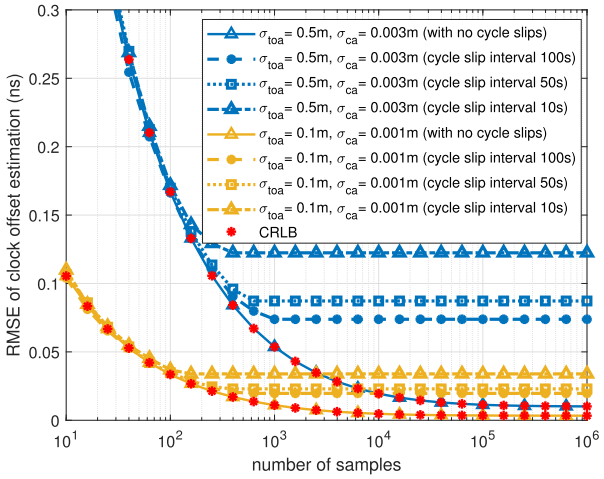

Fig. 6. Clock offset estimation accuracy of the proposed approach under different cycle slip conditions.

As shown in Figs. 4 and 5, with the lower STD of the ToA-based distance measurements, the RMSE of the ToA-based clock offset estimation method is lower, and the RMSE of the proposed CPoA-based method is also better before it converges. With the increasing number of samples, the RMSE of the CPoA-based method converges to the CRLB. The value of the convergent RMSE depends on the STD of the CPoA-based distance measurements, and the lower STD can lead to a better convergent RMSE performance.

We proceed to show the RMSE of the clock offset estimation in the presence of cycle slips. As shown in Fig. 6, the RMSE is larger in the presence of the cycle slips than it is in the absence of cycle slips. Nevertheless, the synchronization accuracy is still about a hundred picoseconds, even when the clip slips occur as frequently as an average of one cycle slip every 10 seconds. It is also observed that, with increasingly frequent cycle slips, the clock offset estimation accuracy of the proposed algorithm degrades, as the consequence of the increasing number of undetected and imperfectly corrected cycle slips.

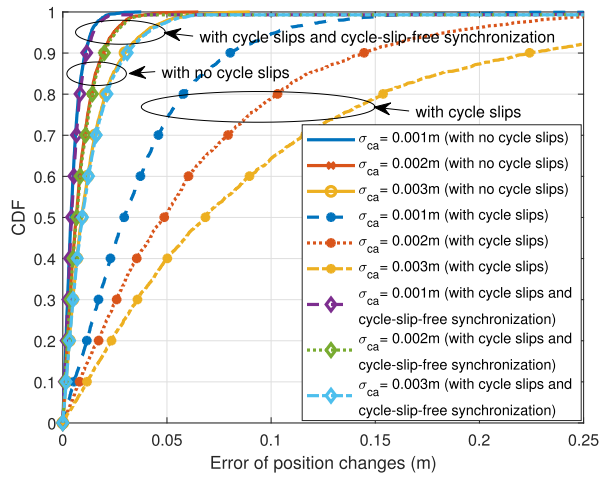

Fig. 7. Estimation accuracy of position changes based on the CPDoA-based distance difference measurements (and TDoA-based estimation of the initial position).

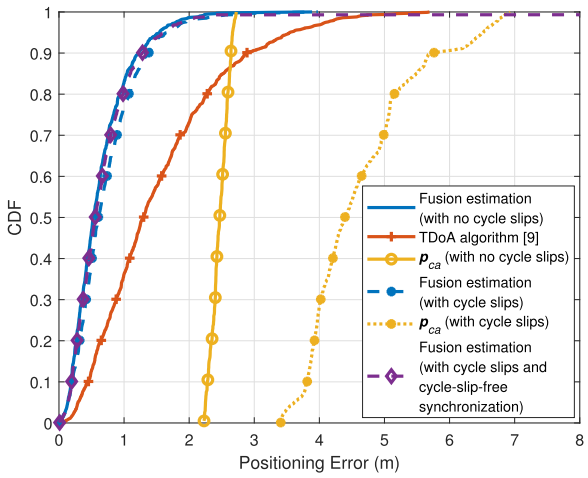

Fig. 8. Performance comparison of the considered different methods for positioning.

B. CPDoA-Based Estimation of MS Position Changes

The estimation accuracy of the MS position changes is evaluated under different STDs of the ToA- and CPoA-based distance measurements, as shown in Fig. 7. The initial point $\hat{\boldsymbol{\theta}}(0)$ is estimated with the algorithm developed in [9], based on the TDoA-based distance difference measurements with the STD of $0.5\mathrm{m}$. In the absence of cycle slips, we observe that high-accuracy estimation of the position changes is achieved, where 90% of the estimation errors are smaller than $0.031\mathrm{m}$.

In the presence of cycle slips, 90% of the estimation errors of the MS position changes are smaller than $0.223\mathrm{m}$, where the average interval between cycle slips is 100 seconds. In particular, when the CPoA-based distance measurements between the BSs are free of cycle slips, the estimation accuracy of the MS position changes is almost the same with and without cycle slips over the links from the MS to the BSs. When the CPoA-based distance measurements between the BSs also experience cycle slips, the estimation accuracy degrades, resulting from the reduced accuracy of the clock offset estimation between the BSs.

C. Position Fusion of ToA-Based Position and CPDoA-Based Position Change Estimations

The fusion-based positioning, i.e., Algorithm 1, is shown in Fig. 8, where the STDs of the ToA- and CPoA-based distance difference measurements are $0.5\mathrm{m}$ and $0.003\mathrm{m}$, respectively. $w_{td} = 0.3$. We observe that the proposed fusion-based position estimation method greatly enhances the positioning accuracy, as compared to positioning only based on the TDoA-based measurements or the ambiguous CPDoA-based measurements. In the presence of cycle slips, the positioning accuracy degrades primarily due to the cycle slips over the links between the BSs and the consequently reduced clock offset estimation of the BSs. The positioning performance of the proposed fusion-based estimation is plotted under different values of w_{td} in Fig. 9, where the estimation variance of $\mathbf{p}_f(t)$ diminishes over time. A smaller w_{td} value leads the positioning error to converge to a smaller value with a growing number of samples, while a larger w_{td} can achieve faster convergence. The cycle slips (over all the links between the BSs and from the MS to the BSs) are shown to have a marginal impact on the convergence of the fusion-based position estimation. In the following simulations, we set w_{td} to 0.3 for the fast convergence of the proposed method.

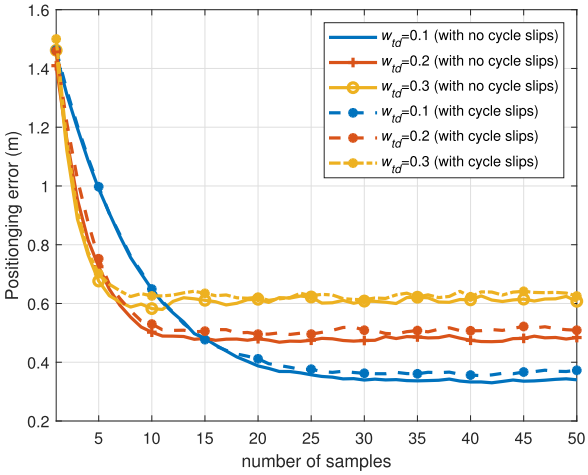

Fig. 9. Positioning error of fusion-based estimation method under different w_{td}.

D. Error Performance of Integer Ambiguity Resolution

We evaluate the accuracy of the integer ambiguity resolution under different STDs of the ToA-based and CPoA-based distance measurements, as shown in Figs. 10 and 11. The accuracy is measured by the average error of integer ambiguity resolution (EoI), as given by

$$EoI = \frac{\|\mathbf{N}^* - \mathbf{N}_{real}\|_0}{M-1}, \tag{52}$$

where $\mathbf{N}_{real}$ collects the ground truth of the integer ambiguities over all the links from the MS to the BSs; and $\|\cdot\|_0$ stands for l_0 norm, i.e., counting non-zero elements.

The probability distributions of EoI are plotted under different STDs of ToA-based distance measurements in Fig. 10, where the x-axis, e.g., "0-1", indicates that the EoI is within $[0, 1)$. The STD of the CPoA-based distance measurements is $0.003\mathrm{m}$. In the absence of cycle slips, the EoI is smaller than 2 cycles in most cases and more than 96% of the EoIs are less than 6 cycles. In the presence of cycle slips, more than 95%

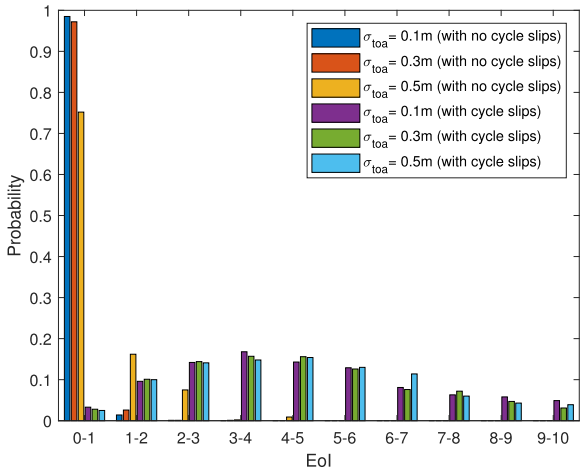

Fig. 10. The probability distributions of EoI under different STDs of the ToA-based distance measurement errors, where the STD of the CPoA-based distance measurements errors is $0.003\mathrm{m}$.

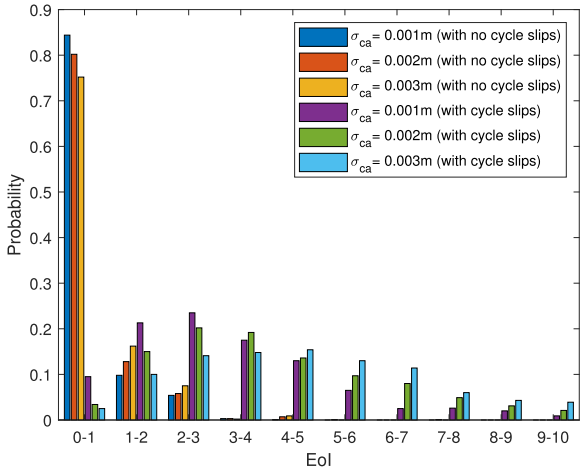

Fig. 11. The probability distributions of EoI under different STDs of the CPoA-based distance measurement errors, where the STD of the ToA-based distance measurement errors is $0.5\mathrm{m}$.

of the EoIs are less than 10 cycles. Additionally, different STDs of the ToA-based distance measurements have impact on the accuracy of the proposed fusion-based estimation of the MS positions, $\mathbf{p}_f(t)$, which in turn affects the accuracy of the linearization and resolution of the integer ambiguities.

The probability distributions of EoI are also plotted under different STDs of the CPoA-based distance measurements in Fig. 11, where the STD of the ToA-based distance measurements is $0.5\mathrm{m}$. In the absence of cycle slips, the EoI is less than 2 cycles in most cases and over 96% of the EoIs are less than 6 cycles. In the presence of cycle slips, more than 95% of the EoIs are less than 10 cycles. The results indicate that the proposed algorithm can cope well with the cycle slips, and resolve the integer ambiguities of the CPDoA-based measurements.

E. Positioning Accuracy Performance

Last but not least, we evaluate the final accuracy of the carrier phase positioning after the integer ambiguity resolution. The cumulative distribution functions (CDFs) of the positioning errors are plotted in Fig. 12. Over 90% of the final positioning errors of the proposed approach are smaller than $0.065\mathrm{m}$

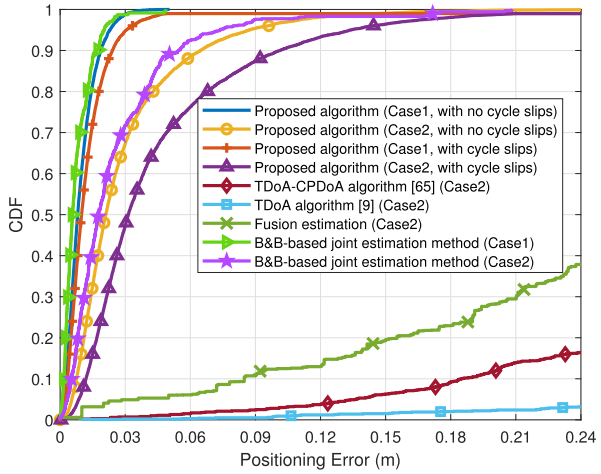

Fig. 12. The positioning accuracy of the proposed carrier phase positioning algorithm (after integer ambiguity resolution) in comparison with its reduced version and existing approaches developed (Case1: $\sigma_{toa} = 0.1\mathrm{m}, \sigma_{ca} = 0.001\mathrm{m}$; Case2: $\sigma_{toa} = 0.5\mathrm{m}, \sigma_{ca} = 0.003\mathrm{m}$).

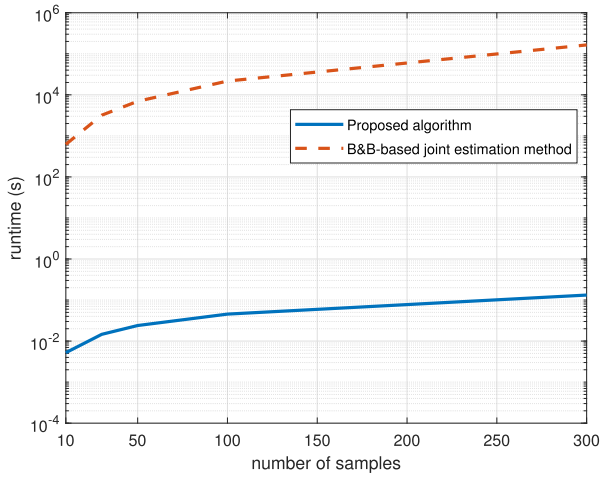

Fig. 13. The comparison of MATLAB runtime between the proposed carrier phase positioning algorithm and the joint estimation method, where the simulations are conducted on a workstation with 3.79GHz CPU and 32GB memory, and the B&B-based joint estimation algorithm is implemented by using MATLAB OPTI toolbox.

in the absence of cycle slips, and smaller than $0.102\mathrm{m}$ in the presence of cycle slips. The proposed positioning method markedly outperforms a recently published TDoA-CPDoA algorithm [65], and the proposed fusion-based position estimation, i.e., Algorithm 1. Despite outperforming the algorithm based on TDoA measurements, the TDoA-CPDoA algorithm [65] and the proposed fusion-based position estimation do not resolve the integer ambiguity. As a consequence, their positioning accuracies are substantially worse than the full proposed approach depicted in Fig. 3. In Fig. 12, we also simulate the joint estimation method which solves problem (8) directly by using the B&B method in MATLAB OPTI toolbox. Under different STDs of the ToA- and CPoA-based distance measurements, both the proposed decoupled and the joint methods can achieve high positioning accuracies with a marginal performance gap, i.e., less than $0.003\mathrm{m}$ on average, despite the dramatically lower complexity of the proposed decoupled algorithm by about six orders of magnitude, as shown in Fig. 13.

VII. Conclusion

In this paper, we proposed a new and accurate carrier phase positioning technique for 5G new radio cellular networks. Firstly, a carrier phase based clock offset estimation method was developed to achieve picosecond-level clock synchronization among BSs. The method was proved to converge to the CRLB asymptotically. Secondly, the temporal changes of the CPDoA-based distance difference measurements were used to estimate the MS position changes at a centimeter-level accuracy, which are insusceptible to the inherent integer ambiguities of the carrier phase measurements. Thirdly, we fused the TDoA positioning results and the estimated position changes, to estimate the MS positions with sub-meter accuracy. Finally, the integer ambiguities were resolved by linearizing the carrier phase measurements, and centimeter positioning accuracies were achieved based on the disambiguated measurements. Simulation results confirmed the feasibility of the proposed carrier phase positioning in wireless cellular networks.

References

[1] J. A. del Peral-Rosado, R. Raulefs, J. A. López-Salcedo, and G. Seco-Granados, "Survey of cellular mobile radio localization methods: From 1G to 5G," *IEEE Commun. Surveys Tuts.*, vol. 20, no. 2, pp. 1124–1148, 2nd Quart., 2018.

[2] Y. Liu, X. Shi, S. He, and Z. Shi, "Prospective positioning architecture and technologies in 5G networks," *IEEE Netw.*, vol. 31, no. 6, pp. 115–121, Nov./Dec. 2017.

[3] E. Y. Menta, N. Malm, R. Jantti, K. Ruttik, M. Costa, and K. Leppanen, "On the performance of AoA–based localization in 5G ultra–dense networks," *IEEE Access*, vol. 7, pp. 33870–33880, 2019.

[4] J. Talvitie, T. Levanen, M. Koivisto, T. Ihalainen, K. Pajukoski, and M. Valkama, "Positioning and location-aware communications for modern railways with 5G new radio," *IEEE Commun. Mag.*, vol. 57, no. 9, pp. 24–30, Sep. 2019.

[5] J. Yan, C. C. J. M. Tiberius, G. J. M. Janssen, P. J. G. Teunissen, and G. Bellusci, "Review of range-based positioning algorithms," *IEEE Aerosp. Electron. Syst. Mag.*, vol. 28, no. 8, pp. 2–27, Aug. 2013.

[6] J. M. Rocamora, I. W.-H. Ho, W. Mak, and A. P. Lau, "Survey of CSI fingerprinting-based indoor positioning and mobility tracking systems," *IET Signal Process.*, vol. 14, no. 7, pp. 407–419, Sep. 2020.

[7] L. Gui, B. He, F. Xiao, and F. Shu, "Resolution limit of positioning error for range-free localization schemes," *IEEE Syst. J.*, vol. 14, no. 2, pp. 2980–2989, Jun. 2020.

[8] K. W. Cheung, H. C. So, W.-K. Ma, and Y. T. Chan, "Least squares algorithms for time-of-arrival-based mobile location," *IEEE Trans. Signal Process.*, vol. 52, no. 4, pp. 1121–1130, Apr. 2004.

[9] Y. T. Chan and K. C. Ho, "A simple and efficient estimator for hyperbolic location," *IEEE Trans. Signal Process.*, vol. 42, no. 8, pp. 1905–1915, Aug. 1994.

[10] N. Xia and M. A. Weitnauer, "TDOA-based mobile localization using particle filter with multiple motion and channel models," *IEEE Access*, vol. 7, pp. 21057–21066, 2019.

[11] Y. Zou, H. Liu, W. Xie, and Q. Wan, "Semidefinite programming methods for alleviating sensor position error in TDOA localization," *IEEE Access*, vol. 5, pp. 23111–23120, 2017.

[12] Z. Su, G. Shao, and H. Liu, "Semidefinite programming for NLOS error mitigation in TDOA localization," *IEEE Commun. Lett.*, vol. 22, no. 7, pp. 1430–1433, Jul. 2018.

[13] W. Wang, G. Wang, F. Zhang, and Y. Li, "Second-order cone relaxation for TDOA-based localization under mixed LOS/NLOS conditions," *IEEE Signal Process. Lett.*, vol. 23, no. 12, pp. 1872–1876, Dec. 2016.

[14] A. Gaber and A. Omar, "A study of TDOA estimation using matrix pencil algorithms and IEEE 802.11ac," in *Proc. Ubiquitous Positioning, Indoor Navigat., Location Based Service (UPINLBS)*, Oct. 2012, pp. 1–8.

[15] Y.-Y. Li, G.-Q. Qi, and A.-D. Sheng, "Performance metric on the best achievable accuracy for hybrid TOA/AOA target localization," *IEEE Commun. Lett.*, vol. 22, no. 7, pp. 1474–1477, Jul. 2018.

[16] X. Guo, N. Ansari, F. Hu, Y. Shao, N. R. Elikplim, and L. Li, "A survey on fusion-based indoor positioning," *IEEE Commun. Surveys Tuts.*, vol. 22, no. 1, pp. 566–594, 1st Quart., 2020.

[17] L. Taponecco, A. A. D'Amico, and U. Mengali, "Joint TOA and AOA estimation for UWB localization applications," *IEEE Trans. Wireless Commun.*, vol. 10, no. 7, pp. 2207–2217, Jul. 2011.

[18] A. Gaber and A. Omar, "A study of wireless indoor positioning based on joint TDOA and DOA estimation using 2-D matrix pencil algorithms and IEEE 802.11ac," *IEEE Trans. Wireless Commun.*, vol. 14, no. 5, pp. 2440–2454, May 2014.

[19] F. Bellili, S. B. Amor, S. Affes, and A. Ghrayeb, "Maximum likelihood joint angle and delay estimation from multipath and multicarrier transmissions with application to indoor localization over IEEE 802.11ac radio," *IEEE Trans. Mobile Comput.*, vol. 18, no. 5, pp. 1116–1132, May 2018.

[20] X. Li and K. Pahlavan, "Super-resolution TOA estimation with diversity for indoor geolocation," *IEEE Trans. Wireless Commun.*, vol. 3, no. 1, pp. 224–234, Jan. 2004.

[21] S. Gezici *et al.*, "Localization via ultra-wideband radios: A look at positioning aspects for future sensor networks," *IEEE Signal Process. Mag.*, vol. 22, no. 4, pp. 70–84, Jul. 2005.

[22] E. D. Kaplan and C. Hegarty, *Understanding GPS/GNSS: Principles and Applications*. Norwood, MA, USA: Artech House, 2017.

[23] P. Axelrad, C. J. Comp, and P. F. Macdoran, "SNR-based multipath error correction for GPS differential phase," *IEEE Trans. Aerosp. Electron. Syst.*, vol. 32, no. 2, pp. 650–660, Apr. 1996.

[24] J. Mo, Z. Deng, B. Jia, H. Jiang, and X. Bian, "A novel FLL-assisted PLL with fuzzy control for TC-OFDM carrier signal tracking," *IEEE Access*, vol. 6, pp. 52447–52459, 2018.

[25] B. Geoffrey, *Basics of the GPS Technique: Observation Equations*. Stockholm, Swedish: Swedish Land Survey, 1997.

[26] Y. Zhao, "Applying time-differenced carrier phase in nondifferential GPS/IMU tightly coupled navigation systems to improve the positioning performance," *IEEE Trans. Veh. Technol.*, vol. 66, no. 2, pp. 992–1003, Feb. 2017.

[27] A. A. López-Salcedo, J. A. Del Peral-Rosado, and G. Seco-Granados, "Survey on robust carrier tracking techniques," *IEEE Commun. Surveys Tuts.*, vol. 16, no. 2, pp. 670–688, 2nd Quart., 2014.

[28] M. Petovello *et al.*, "Carrier phase and its measurement for GNSS," *Inside GNSS*, vol. 5, no. 5, pp. 18–22, 2010.

[29] M. Petovello, "Why are carrier phase ambiguities integer," *Inside GNSS*, vol. 2015, pp. 36–38, Jan. 2015.

[30] H. Dekkiche, S. Kahlouche, and H. Abbas, "Differential ionosphere modelling for single-reference long-baseline GPS kinematic positioning," *Earth, Planets Space*, vol. 62, no. 12, pp. 915–922, 2010.

[31] C. C. Goad, "Short distance GPS models," in *GPS for Geodesy*. Berlin, Germany: Springer, 1996, pp. 239–262.

[32] H. Qin, P. Liu, L. Cong, and W. Ji, "Triple-frequency combining observation models and performance in precise point positioning using real BDS data," *IEEE Access*, vol. 7, pp. 69826–69836, 2019.

[33] X. Gu and B. Zhu, "An improved ambiguity resolution of three carriers in precise point positioning," *IEEE Access*, vol. 6, pp. 3951–3961, 2018.

[34] Z. Pan, H. Chai, and Y. Kong, "Integrating multi-GNSS to improve the performance of precise point positioning," *Adv. Space Res.*, vol. 60, no. 12, pp. 2596–2606, Dec. 2017.

[35] CATT, *Discussion of Potential Techniques for NR Positioning*, document 3GPP R1-1810532, Oct. 2018.

[36] CATT, *Discussion of NR Positioning Enhancements*, document 3GPP R1-2005712, Aug. 2020.

[37] 3GPP, *Physical Channels and Modulation*, document 3GPP TR 36.211, Jun. 2021.

[38] 3GPP, *Study on NR Positioning Support*, document 3GPP TR 38.855, Mar. 2019.

[39] J. Palacios, P. Casari, and J. Widmer, "JADE: Zero-knowledge device localization and environment mapping for millimeter wave systems," in *Proc. IEEE Conf. Comput. Commun. (IEEE INFOCOM)*, May 2017, pp. 1–9.

[40] 3GPP, *Study on Channel Model for Frequencies From 0.5 to 100 GHz*, document 3GPP TR 38.901, Jan. 2020.

[41] G. Xu and Y. Xu, "Applications of GPS theory and algorithms," in *GPS: Theory, Algorithms and Applications*. Berlin, Germany: Springer, 2016, pp. 313–340.

[42] Z. Chaloupka, "Technology and standardization gaps for high accuracy positioning in 5G," *IEEE Commun. Standards Mag.*, vol. 1, no. 1, pp. 59–65, Mar. 2018.

[43] J. A. del Peral-Rosado, J. A. Lopez-Salcedo, G. Seco-Granados, P. Crosta, F. Zanier, and M. Crisci, "Downlink synchronization of LTE base stations for opportunistic ToA positioning," in *Proc. Int. Conf. Location GNSS (ICL-GNSS)*, Jun. 2015, pp. 1–6.
[44] M. Panchetti, C. Carbonelli, M. Horvat, and M. Luise, "Performance analysis of PRS-based synchronization algorithms for LTE positioning applications," in *Proc. 10th Workshop Positioning, Navigat. Commun. (WPNC)*, Mar. 2013, pp. 1–6.
[45] M. Koivisto *et al.*, "Joint device positioning and clock synchronization in 5G ultra-dense networks," *IEEE Trans. Wireless Commun.*, vol. 16, no. 5, pp. 2866–2881, May 2017.
[46] S. M. Kay, "Fundamentals of statistical signal processing: Estimation theory," in *Technometrics*. Upper Saddle River, NJ, USA: Prentice-Hall, Nov. 1995.
[47] Y. Shen, H. Wymeersch, and M. Z. Win, "Fundamental limits of wideband localization—Part II: Cooperative networks," *IEEE Trans. Inf. Theory*, vol. 56, no. 10, pp. 4981–5000, Oct. 2010.
[48] H. L. V. Trees, *Detection, Estimation, and Modulation Theory, Part IV, Optimum Array Processing*. Hoboken, NJ, USA: Wiley, 2004.
[49] B. Feng, M. Fu, H. Ma, Y. Xia, and B. Wang, "Kalman filter with recursive covariance estimation—Sequentially estimating process noise covariance," *IEEE Trans. Ind. Electron.*, vol. 61, no. 11, pp. 6253–6263, Nov. 2014.
[50] M. Karasalo and X. Hu, "An optimization approach to adaptive Kalman filtering," *Automatica*, vol. 47, no. 8, pp. 1785–1793, Aug. 2011.
[51] M. Sahmoudi and R. Landry, "A nonlinear filtering approach for robust multi-GNSS RTK positioning in presence of multipath and ionospheric delays," *IEEE J. Sel. Topics Signal Process.*, vol. 3, no. 5, pp. 764–776, Oct. 2009.
[52] L. Zhenkun and H. Shunji, "Research on ambiguity resolution aided with triple difference," *J. Syst. Eng. Electron.*, vol. 19, no. 6, pp. 1090–1096, Dec. 2008.
[53] C. Gunther and P. Henkel, "Integer ambiguity estimation for satellite navigation," *IEEE Trans. Signal Process.*, vol. 60, no. 7, pp. 3387–3393, Jul. 2012.
[54] Y. Wang *et al.*, "Non-data-aided cycle slip self-correcting carrier phase estimation for QPSK modulation format of coherent wireless optical communication system," *IEEE Access*, vol. 7, pp. 110451–110462, 2019.
[55] L. Yin, S. Li, Z. Deng, and D. Zhu, "A novel cycle slips detection model for the high precision positioning," *IEEE Access*, vol. 7, pp. 24041–24050, 2019.
[56] U. Beitler and O. Amrani, "Real time cycle slip detection and correction for APSK modulation," *IEEE Trans. Commun.*, vol. 62, no. 2, pp. 736–746, Feb. 2014.
[57] S. S. Arslan, J. Lee, and T. Goker, "Cycle slip detection and correction through classification of modulation code failures," *IEEE Trans. Magn.*, vol. 49, no. 9, pp. 4988–4998, Sep. 2013.
[58] H. Hu and L. Fang, "GPS cycle slip detection and correction based on high order difference and Lagrange interpolation," in *Proc. 2nd Int. Conf. Power Electron. Intell. Transp. Syst. (PEITS)*, Dec. 2009, pp. 1–4.
[59] K. Berntorp, A. Weiss, and S. D. Cairano, "Integer ambiguity resolution by mixture Kalman filter for improved GNSS precision," *IEEE Trans. Aerosp. Electron. Syst.*, vol. 56, no. 4, pp. 3170–3181, Aug. 2014.
[60] N. Nadarajah, P. J. G. Teunissen, and N. Raziq, "Instantaneous GPS–Galileo attitude determination: Single-frequency performance in satellite-deprived environments," *IEEE Trans. Veh. Technol.*, vol. 62, no. 7, pp. 2963–2976, Sep. 2013.
[61] A. Brack, "Long baseline GPS+BDS RTK positioning with partial ambiguity resolution," in *Proc. Int. Tech. Meeting Inst. Navigat.*, Mar. 2017, pp. 754–762.
[62] F. Shen, D. Xu, and P. Zhao, "Study on carrier tracking performance of DS/BPSK navigation receiver in the multipath environment," in *Proc. 4th Int. Conf. Wireless Commun., Netw. Mobile Comput.*, Oct. 2008, pp. 1–5.
[63] A. Shahmansoori, B. Uguen, G. Destino, G. Seco-Granados, and H. Wymeersch, "Tracking position and orientation through millimeter wave lens MIMO in 5G systems," *IEEE Signal Process. Lett.*, vol. 26, no. 8, pp. 1222–1226, Aug. 2019.
[64] L. Chen, W. Qi, E. Yuan, and Y. Zhao, "Joint 2-D DOA and TOA estimation for multipath OFDM signals based on three antennas," *IEEE Commun. Lett.*, vol. 22, no. 2, pp. 324–327, Feb. 2018.
[65] H. Chen, T. Ballal, N. Saeed, M.-S. Alouini, and T. Y. Al-Naffouri, "A joint TDOA-PDOA localization approach using particle swarm optimization," *IEEE Wireless Commun. Lett.*, vol. 9, no. 8, pp. 1240–1244, Aug. 2020.

Shaoshuai Fan (Member, IEEE) received the M.S. degree in information and communication engineering from Jilin University, Changchun, China, in 2009, and the Ph.D. degree in communication and information system from Beijing University of Posts and Telecommunications (BUPT), Beijing, China, in 2015.

From 2015 to 2017, he was a Post-Doctoral Researcher with BUPT, where he is currently a Lecturer. His current research interests include networking technologies for 5G and beyond, localization theory and technologies, and mobile edge caching.

Wei Ni (Senior Member, IEEE) received the B.E. and Ph.D. degrees in communication science and engineering from Fudan University, Shanghai, China, in 2000 and 2005, respectively.

From 2005 to 2008, he was a Post-Doctoral Research Fellow at Shanghai Jiaotong University; a Deputy Project Manager at Bell Labs, Alcatel/Alcatel-Lucent, from 2005 to 2008; and a Senior Researcher at the Division of Devices Research and Development, Nokia, from 2008 to 2009. Currently, he is a Group Leader and a Principal Research Scientist at CSIRO, Sydney, Australia; an Adjunct Professor at the University of Technology Sydney; and a Honorary Professor at Macquarie University. He has authored five book chapters, more than 200 journal articles, more than 80 conference papers, 25 patents, and ten standard proposals accepted by IEEE. His research interests include machine learning, online learning, stochastic optimization, and their applications to system efficiency and integrity. He has been the Chair of IEEE Vehicular Technology Society (VTS) New South Wales (NSW) Chapter since 2020 and an Editor of IEEE TRANSACTIONS ON WIRELESS COMMUNICATIONS since 2018. He served as the Secretary and then the Vice-Chair for IEEE NSW VTS Chapter from 2015 to 2019, the Track Chair for 2017 VTC-Spring, the Track Co-Chair for 2016 IEEE VTC-Spring, the Publication Chair for 2015 BodyNet, and the Student Travel Grant Chair for WPMC 2014.

Hui Tian (Senior Member, IEEE) received the M.S. degree in microelectronics and the Ph.D. degree in circuits and systems from Beijing University of Posts and Telecommunications (BUPT), Beijing, China, in 1992 and 2003, respectively. She is currently a Professor with BUPT, where she is also the Network Information Processing Research Center Director of the State Key Laboratory of Networking and Switching Technology. Her current research interests include radio resource management, mobile-edge computing, Industrial Internet of Things, and mobile social networks.

Zhiqian Huang received the B.E. and M.S. degrees from Beijing University of Posts and Telecommunications (BUPT), Beijing, China, in 2017 and 2020, respectively. His research interests include wireless communication and wireless positioning.

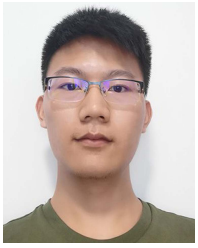

Rengui Zeng received the B.E. degree from Beijing University of Posts and Telecommunications (BUPT) in June 2019, where he is currently pursuing the M.E. degree with the State Key Laboratory of Networking and Switching Technology. His research interests include wireless communication and wireless positioning.